A Bucciarelli, T Muthukumar, JS Kim, WK Kim, A Quaranta, D Maniglio, G. Khang, A. Motta
Preparation and Statistical Characterization of Tunable Porous Sponge Scaffolds using UV Cross-linking of Methacrylate-Modified Silk Fibroin
ACS Biomaterials Science and Engineering,12, 6374-6388, 2019
10.1021/acsbiomaterials.9b00814

Preparation of a porous solid fibroin scaffold based on a foaming and UV crosslinking procedure of a methacrylate fibroin solution: evaluation of the influence of the composition on the sponge properties.

Alessio Bucciarelli*[1,2,3], Muthukumar Thangavelu[4], Jin Su Kim[4], Won Kyung Kim[4], Alberto Quaranta[1], Devid Maniglio[1,2], Gilson Khang[4], Antonella Motta[1,2]

[1] Department of Industrial Engineering, University of Trento, via Sommarive 9, Trento, Italy.

[2] BIOTech Research Center, University of Trento, via delle Regole 101, Trento, Italy and European Institute of Excellence on Tissue Engineering and Regenerative Medicine, Trento, Italy.

[3] Microsystems technology group, Fondazione Bruno Kessler, via Sommarive 18, Trento, Italy.

[4] Department of BIN Convergence Technology, Department of Polymer Nano Science & Technology and Polymer Materials Fusion Research Center, Chonbuk National University, Deokjin-gu, Jeonju 561-756, Republic of Korea.

Abstract

Silk fibroin scaffolds have been widely studied in literature and several fabrication methods have been proposed. Most of these procedures are based on the secondary structure transition of the protein to the stable β crystalline form. This transition, known as physical crosslinking, makes the sponge resistant to the dissolution in water, and, in general increases the sponge stiffness. In our work, we propose an alternative method, to ensure the stability of the sponge, based on a chemical crosslink. This process uses a methacrylated version of silk fibroin (Fibroin-MA) obtained via chemical modification. The water solution of this protein with the addition of a photoinitiator (LAP) allows the opening under the UV light of the double carbon-carbon bond and the radical polymerization. The incorporation of air bubble that serves as template was accomplished by the use of a mixer, then the foam was stabilized under UV light and the excess of water removed by freeze drying. The functionalization of the protein was confirmed by FTIR analysis. To evaluate the effect of the composition on the sponge properties a 2^3 full factorial

design of experiment has been adopted. The FTIR analysis revealed that the sponge composition did not affect the protein secondary structure. The analysis of images obtained by SEM allowed to study and model some statistical measures of the porosity curves. The same modeling procedure was applied to the dissolution test in a simulated body fluid, to the water absorption, and to the cell viability (evaluated by the MTT assay). An empirical model for each property was build, demonstrating how changing the composition is possible to tune the sponge properties.

Introduction

Silk fibroin sponges have been extensively studied in the literature, in particular in all the applications in which porosity is an essential feature. In tissue engineering, porous structures of the material serves to closely mimic the biological microenvironment. Porous fibroin sponges have been successfully adopted in the case of soft tissues (muscle, skin, adipose, and neural tissues) and bones[1–4]. To produce an efficient scaffold different parameter are essential. In order to mimic the living tissues, the porosity should be open and tunable, the mechanical stiffness should be adjusted according to the treated tissue and the sponge should be stable in water[5–8]. Plenty of different methods were developed to produce silk fibroin sponges, among them: salt-leaching[9–12], freeze drying[13–16], freeze-thaw treatment[17], ammonium bicarbonate sublimation[18], self-assembly[19], and NO_2 expansion[20]. All these methods are based on the transition of the protein secondary structure from random coil to a crystalline β-sheet structure that makes the sponge stable in water. This transition, known as physical crosslinking, can be performed both with a post-production treatment as water annealing or the immersion in methanol or ethanol or using a method that produces by itself a stable crystalline sponge as for instance the NO_2 expansion[20]. However, the physical crosslinking is a change in the protein configuration and is less stable then a chemical crosslinking in which the stability is ensured by the formation of a 3D continuous network. Once the protein is in its β-form it could always be denatured by solutions able to break the h-bond between the β-

strands. A chemical crosslinking of the protein can be obtained by two approaches. The first one consists in promoting the formation of dytirosine and trityrosine crosslinking, for instance the use of metal complexes and electron acceptors (ruthenium and ammonium persulphate and UV irradiation)[21], vitamin (riboflavin and UVA irradiation)[22], enzymes in combination with a chemical activation (hydrogen peroxide and horseradish peroxidase)[23–26]. The latter consists in the use of a chemical modified version of the original protein, in which vinyl groups are added as sides groups in the protein chain through a chemical reaction and then initializing the radical formation and propagation by UV exposure. Both approaches allowed to obtain a stable crosslinking. However, among them, independently of the typology of crosslink made (by linking tyrosine or vinyl groups), the methods that are photoinitiated allow to initiate the reaction and stop it just by controlling the irradiation. This is a great advantage in comparison to enzymatic systems in which the reaction occurs with time. For our method we decided to modify the fibroin protein by chemical modification. At least two different reactions can be used to perform this modification. The first and oldest approach implies the use of an isocyanate (2-Isocyanatoethyl methacrylate, IEM), and an organic solvent (dimethyl sulfoxide, DMSO), to obtain a fibroin photoresist (fibroin photocrosslinkable photoresist, FPP)[27–30] not water soluble. In this case due to the high reactivity of the isocyanate different side groups were reported to be modified: mainly hydroxy groups (Ser, Ter, Thr) and in minor extent amino group (lys)[31]. In the second and more recent method where the chemical reaction with the protein was conducted using glycidyl methacrylate (2,3-Epoxypropyl methacrylate, GMA) in water, to obtain a bioink[32] (methacrylated silk, sil-MA) in water solution. Here the modification took place in the amine (NH_2) side group of lysine as proved by magnetic nuclear resonance (NMR)[32]. Sil-Ma has been used to produce hydrogel objects by digital light processing (DLP) printing. On the resulting material an accurate characterization has been performed However none of studied the properties, reported to be tunable with the degree of methacrylation, was statistically modeled, with the result of a lack of standardization and controllability. In this study, using the previously developed Sil-

MA, we proposed a simple and innovative method to produce a chemically crosslinked silk fibroin sponge with controllable porosity, mechanical proprieties, and stability in water. A foam is initially produced from the aqueous solution of Fibroin-MA by incorporating air using a mixer. The addition of a photoinitiator and the successive UV exposure allow the radical polymerization to take place opening the double carbon bonds, forming a 3D network and stabilizing the foam. In the final step the water removal was done to obtain the final sponge achieved by freeze drying. Design of experiment (DOE) is widely used statistical methodology to standardize and optimize processes in the industrial production[33]. It allows to understand which parameters have an impact on the product properties. In our case we decided to use the DOE method to understand the how the different component of the sponge composition influenced the material properties. In particular, instead of using the convention approach of modifying the process parameters, the process was kept constant and 3 factors of the sponge composition were considered: the protein concentration in solution, the percentage of photoinitiator, and the addition of a surfactant. The resultant sponges were analyzed and through DOE an empirical model for each studied property was built. The porosity, the water absorption, the dissolution in a simulated body fluid (SBF), the compressive young modulus and the cytotoxicity were evaluated and modeled with a confidence interval of 95%. Using our method, we proved the possibility to tune the porosity and its dispersion as much as the sponge mechanical and chemical stability just by changing the initial composition. This could constitute a platform system to produce different kind of scaffold responding to the necessity of the different tissues to be treated. In addition, the possibility to change also the process parameter could give, with further studies, additional degrees of freedom, and probably an increase in the numerical range in which the considered properties are tunable.

Materials and methods

Silk fibroin preparation

Extraction and purification of silk fibroin was conducted using an adapted version of a well-known protocol[34]. Briefly, to separate silk fibroin from silk sericin, Bombyx mori silk cocoons has been cut in small pieces and placed in a 0.01 M hot bath of sodium carbonate (Na_2CO_3, Sigma Aldrich) for 1 hour, followed by a second bath of sodium carbonate with a concentration of 0.003M for 1 hour. The resultant silk fibroin, progressively taken at room temperature, was carefully rinsed for 3 times using ultrapure water and then dried for 2 days.

Methacrylated silk fibroin (Sil-MA) solution preparation

Fibroin-MA was prepared following a protocol described elsewhere[32]. Briefly, 20 g of the degummed silk fibroin were dissolved into 100 mL of a 9.3 M water solution of lithium bromide (LiBr, Sigma Aldrich) at 60°C for 4 h in an oven. Subsequently, 10 mL of glycidyl methacrylate (GMA, Sigma Aldrich) were added in the solution, that were then stirred at 65°C for 4 h in order to allow the conjunction reaction. To remove the salt and the unreacted GMA, the resulting Sil-MA solution was dialyzed for 4 days against water using a 3.5 kDa dialysis tube. The solution concentration in mg/mL was checked using a spectrophotometer (BioSpectrometer basic, Eppendorf) evaluating the intensity of the A280 protein peak (280 nm). The solution was concentrated (10 or 20 %) evaporating the water at low temperature by the use of a rotavapor (Eyela N-1110AN) at 70°C and 300 rpm, checking the concentration time to time until the desired one was reached. The resultant fibroin – MA water solution was then filtered with a 50 µm glass filter and then stored at 4 °C. In **figure 1** the possible reaction pathway is shown, a previous study demonstrated that the site for the reaction is the amide side group of lysine amino acid[32]. In the reaction a primary amide became a di-β-hydroxyamide, through the nucleophilic substitution of nitrogen on one carbon atom of the epoxy ring and the consequent ring opening[35].

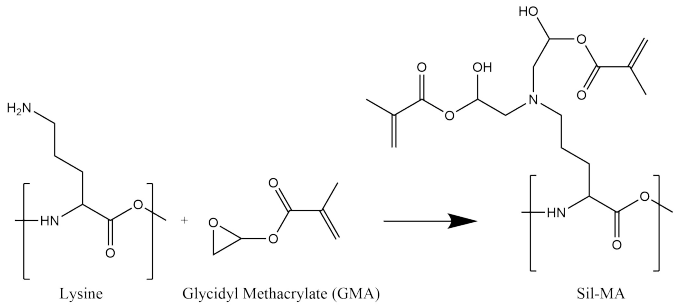

Figure 1: Chemical pathway for the formation of the Sil-MA protein, a primary amide became a di-β-hydroxyamide, through the nucleophilic substitution of nitrogen on one carbon atom of the epoxy ring and the consequent ring opening. The site of reaction as previously reported is the lysine side groups.

Sponge's preparation

We prepared 3 fibroin – MA sponges for each composition shown in **table 1**, for a total of 24 samples. The sponge preparation follows the scheme of **Figure 2A**. In the step 1 (**Figure 2A-1**), based on the sample composition, a certain amount of fibroin - MA solution (5 mL for the 10 % solution and, 2.5 mL for the 20 % solution) was transferred to a 15 mL glass vial, then the photoinitiator, lithium phenyl-2,4,6-trimethylbenzoylphosphinate (LAP, Sigma Aldrich), and the surfactant, Polyethylene glycol sorbitan monolaurate (Tween 20, Sigma Aldrich), were added. In the step 2 (**Figure 2A-2**), the solution was mixed and emulsified using a Bio-gen Pro 200 homogenizer (PRO Scientific) at 35000 rpm for 2.5 m. Immediately after the structure were allowed to crosslink under UV light (SpotLED curing equipment centered at 365 nm, Photo electronics) for 20 min. In the step 3 (**Figure 2A-3**) the product was frozen at -80 °C into an ultra-low freezer for 2 h and lyophilized at -50 °C for 2 days. It should be noted that we choose to keep constant the percentage of protein and not the volume of solution. Each sponge contains 500 mg of fibroin-MA, so accordingly the percentage of photoinitiator can be converted in percentage on protein weight (5 mg equal to 1 % w/w, 75 mg equal to 15 % w/w). The same consideration can be applied to the percentage of surfactant knowing its density (1.1g/mL, 50 µL correspond to 55 mg and then 11 % w/w).

Figure 2B and **2C** highlight the crosslinking mechanism. The methacrylated protein solution is in the denaturated state, the double bonds are freely available (**figure 2B-1**), the addition of air bubble due to the mixing procedure allow the formation of thin layer of protein (**figure 2B-2**) these are stabilized by crosslinking under UV-light (**figure 2B-3**) then the removal of water left and the rupture of bubbles membrane was obtained by freeze drying (**figure 2B-4**). The chemical pathway is shown **in figure 1C** and it was proposed for the crosslinking of the fibroin photoresist (FPP)[36]. The UV light irradiation allow the initial formation of radicals (**figure 2C-1**) due to the bond opening of the photoinitiator (Lithium phenyl-2,4,6-trimethylbenzoylphosphinate, LAP)[37]. The formation of radicals on the protein chain due to the effect of the radicals formed by the photoinitiator (here indicated with R) and the opening of the carbon double bond (**figure 2C-2**). The formation of a crosslinking between two chains, due to the opening of the carbon double bond (**figure 2C-3**).

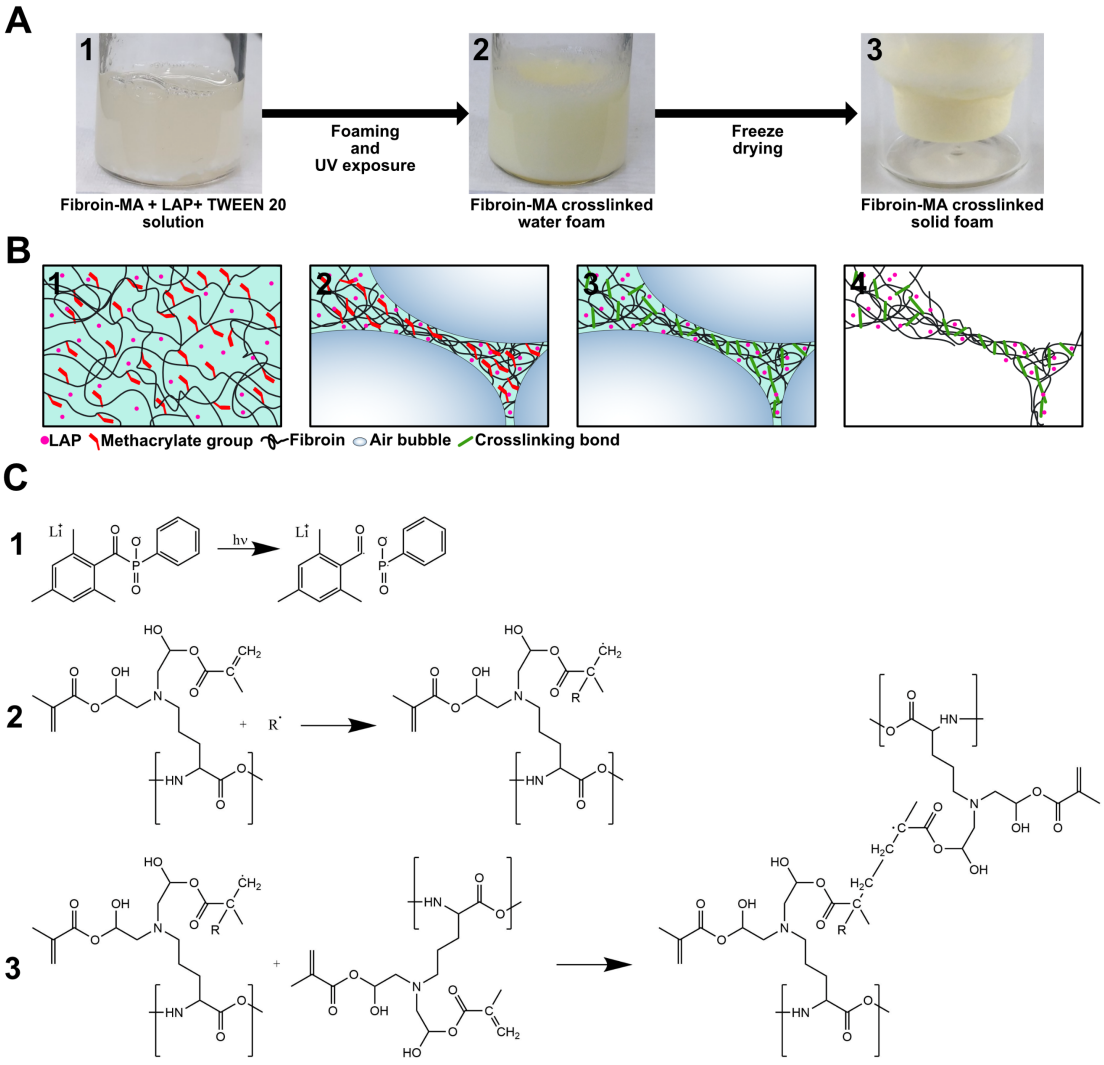

*Figure 2: (**A**) Method for fibroin – MA foam preparation. (**1**) In the fibroin-MA solution the photoinitiator (LAP) and the surfactant (Tween 20) were added. (**2**) The solution was then foamed using a mixer and exposed to a 365 nm UV light to stabilize the structure by chemical crosslinking. (**3**) Finally, to remove the excess of water the foamed solution was frozen at -80°C and then freeze dried to obtain the final material. (**B**) Proposed mechanism of sponge formation. (**1**) The double bond group are attached to the protein chain as side group, in the denatured state of the protein this groups are highly reactive cause no sterical impediment is present. (**2**) Within the formation of the foam thin layer between air bubbles are formed. (**3**) The exposure to UV light ensures the opening of the double bond and the stabilization of the overall structure. (**4**) The freeze-drying ensures the removal of the water leaving the final porous structure. (**C**) The chemical pathway of the reaction. (**1**) The formation of radicals under UV light due to the photoinitiator (Lithium phenyl-2,4,6-trimethylbenzoylphosphinate, LAP). (**2**) The formation of radicals on the protein chain due to the effect of the radicals formed by the photoinitiator (here indicated with R) and the opening of the carbon double bond. (**3**) The formation of a crosslinking between two chains, due to the opening of the carbon double bond.*

Sample Compositions	[Fibroin – MA] %	$V_{Tween20}$ µL	m_{LAP} mg
1	10	0	5
2	20	0	5
3	10	50	5
4	20	50	5
5	10	0	75
6	20	0	75
7	10	50	75
8	20	50	75

Table 1: Composition of the prepared sponges. We choose to vary the percentage of fibroin-MA in solution, the percentage of the surfactant (Tween20) and the percentage of initiator (LAP). Three samples were prepared for each composition.

Lyophilized silk fibroin sponge preparation

The regenerated silk fibroin solution was concentrated to 10% then placed into vials of 15 mL, rapidly frozen using liquid nitrogen, and freeze-dried for 3 days to obtain the lyophilized sponge. Then the sponge was placed in an humidostatic chamber (80% relative humidity, room temperature) for 12 h to allow the water annealing. This sponge was used as comparison for the compressive modulus and the LDH assay.

Structural analysis

Assignment	Peak position cm^{-1}	Reference
Side chain	1597-1609	38–41
Antiparallel β – sheet	1610-1625	38,39,49,40,42–48
Native β – sheet	1626-1636	38,41–47
Random coil	1637-1655	38,41,42,46,48,50
α – helix	1656-1662	38,41,42,46
B – turns	1663-1696	38,40,42,46,47,49,51
Parallel β – sheet	1697-1703	38,46,47,52

Table 2: Peak positions and their secondary structure assignment used for the primary amide fitting.

Structural analysis was conducted by the use of ATR-FTIR (GX Perkin Elmer), collecting 16 spectra in the range 4000 – 400 cm^{-1} range with a resolution of 1 cm^{-1}. To understand if the methacrylation successfully occurred, and its influence on the secondary structure we analyzed four films: two made by the fibroin-MA water solution, one film exposed to UV light (SpotLED curing equipment centered at 365 nm, Photo electronics) to allow the crosslinking, the second not exposed, and two film made by a fibroin water solution, one water annealed for 12 h in a humidostatic chamber (80% relative humidity, room temperature) to allow a physical crosslinking, the other untreated. The secondary structure changes on sponges were evaluated using an ATR-FTIR spectrophotometer (Perkin Elmer, Spectrum ONE). To maximize the signal to noise ratio, 32 spectra with a resolution of 1 cm^{-1} were collected and averaged for each sample. Subsequently, the secondary structures were quantitatively evaluated analyzing the primary amide peak (1580-1720 cm^{-1}). The peak was smoothed with a 5 points adjacent averaging function followed by a Fourier self-deconvolution (FSD, with smoothing factor of 0.3 and gamma function of 30) to enhance the resolution and better shape the singular components. A second derivative of the deconvolved peak was then performed to identify the component positions which were consequently, used to fit the singular peaks with a Gaussian function. The fitting routine was recursively applied until χ^2 was minimized. The ratio between the fitted peak area and the total area was calculated to determine the percentage of the specific structure assigned to the peak. In **table 2,** the assigned secondary structure for different bandwidths of the FTIR spectrum is reported.

Microstructural analysis

The samples porosity was evaluated by SEM (BioLV-SEM, S-3000N, Hitachi): two images at 60 x of magnification were taken for each sample then a threshold limit was imposed in the grayscale and the image analyzed using ImageJ[53,54]. The analysis was conducted following the steps of **figure 3**. Only pores with a closed perimeter were considered. The pore shape was not circular, so we chose to evaluate

the porosity referring to the parameter that can be evaluated directly from the thresholded image: the pore area. The pore detection and measurement were performed by an algorithm, that can include artifact especially in the low region of the porosity distribution. Considering the scale of our image, only pores with a diameter higher than 1/10 of the scale bar were included (approximately 50 µm of diameter and 5000 μm^2 of area) into further calculations. Then the pores median area, the interquartile range (IQR), the mean area, and the standard deviation were calculated and used as the yield for the successive statistical analysis. An equivalent pore diameter was calculated by the strong assumption of circular porosity, using the formula:

$$d = 2 * \frac{\sqrt{A}}{\pi}$$

where A is the estimated area.

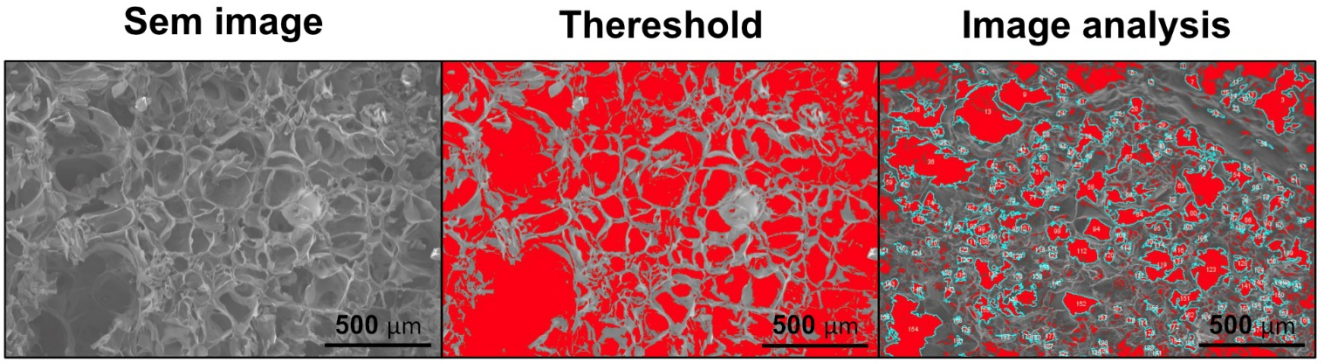

Figure 3: Image analysis for porosity distribution, two SEM images at 60x of magnification were taken for each samples a threshold level were imposed in order to make clear the pore boundaries, finally the area of each closed pore was evaluated.

Water absorption

For each of the 8 compositions, we prepared 3 sponges of equal weight (about 100 mg) for each time point (1, 3, 7, and 14 days). The sponges were weighted directly after the freeze drying to ensure that the weight was not affected by the presence of water. Subsequently, the samples were soaked in 5 mL of simulated body fluid (SBF) at 37 °C inside an incubator. The samples were then removed at the respective time point, rapidly dried with a filter paper and then weighted. The difference between the wet weight

(w_{wet}) and the dry weight (w_{dry}) normalized to the dry weight has been used to report in percentage water adsorption using the following formula:

$$H_2O[\%] = \frac{w_{wet} - w_{dry}}{w_{dry}} * 100$$

Dissolution

The dissolution was evaluated using a spectroscopic method recently reported to be reliable to determine the protein concentration in solution[42]. The concentration in mg/mL of the protein released in the SBF solution was evaluated by the use of a spectrophotometer (BioSpectrometer basic, Eppendorf) using the absorption at 280 nm (A280 protein peak, molar extinction coefficient of 44,700 $cm^{-1}M^{-1}$ [55,56]). The resulting concentration ([rSF]) was then multiplied for the solution volume in mL (5), to obtain the total amount in mg of fibroin present inside the solution. The amount was, then normalized to the initial weight of the sponge (w_{dry}) and reported in percentage using the following formula:

$$m_{rSF}[\%] = \frac{[\mathrm{rSF}] * 5}{w_{dry}} * 100$$

Compression test

Compression tests were performed using a Bose Electroforce 3220 (USA) with a compression rate of 0.5 mm/m in a controlled environment (25 °C and 20% relative humidity). The Young's modulus was evaluated as an angular coefficient of the curve in the initial elastic (linear) zone. For each composition 3 sponges were tested all with a approximately diameter of 8 mm and a thickness of 5 mm.

Preliminary in vitro evaluation: MTT and LDH

In this work NIH 3T3 cell line was used to atusy the cytocompatibility of the sponge. RPMI medium was used to culture and maintain the cell lines. This culture medium was supplemented with 10% fetal bovine serum and 1% antibiotic-antimycotic under standard conditions (37º C in a humidified atmosphere containing 5% CO_2). The 3-(4,5-dimethylthiazol-2-yl)-2,5-diphenyltetrazolium bromide (MTT) assay was carried out to determine the cytocompatibility material and cell viability of NIH 3T3 cells based on the reductive cleavage of MTT to formazan by mitochondrial dehydrogenase of living cells[57]. The cells were seeded at a density of 2×10^5 cells/ scaffold and incubated with RPMI medium for 72 hours at 37°C humidified with 5% CO_2. Three replicates for each sample were incubated and cells cultured with RPMI medium were used as positive control. After 72 hours cell culture medium was replaced by culture medium containing MTT in a 9:1 ratio and incubated for 3 h in dark at 37°C. When violet crystals were formed, they were dissolved using dimethyl sulfoxide solution (DMSO) then the optical density was evaluated at 570 nm using microplate reader. The results were plotted as percentage of the positive control, reporting a mean and a standard deviation, then performig an ANOVA to check if the results were statisticcaly significant in comparison to the control. These data were further analized by DOE to verify if any second order effect influenced the cell viability.

LDH has been performed to verify the effect of the LAP residual. The sponges prepared woth the 10% sil-MA concentration where washed in water for 2 days under agitation at 60 rpm. These sponges were compared with the non washed one, to observe if an addititional washing could favorably impact the citoxicity, lowering it. The extract from substrates was prepared by incubating sponges in a defined volume of reduced medium (w/o phenol red and w/ heat inactivated serum). The volume was calculated according to the standard ISO-10993-12:2004. For irregularly shaped porous devices (low-density materials), the required surface/volume was 0,1 gr/mL. Each sample was then weighted, and the extract volume was calculated accordingly. NIH 3T3 cells were seeded, in the same condition of the previous

test, in 96-well TCP and cultured in the standard medium until about 70% confluence. Subsequentially, cells were exposed for 48 hours to the conditioned medium (120 µl/well). The positive control for cytotoxicity was a fully lysate cells (0.5% Triton X). Negative control consisted of cells cultured in the standard medium. The lactate dehydrogenase reaction mix was prepared following the standard protocol assay reported by the manufacturer's instructions. 50 µL of each sample medium were transferred to a 96 well-plate, and 50 µL of reaction mix were added to each well and gently mixed. The plate was then covered with an opaque material in order to protect it from light and incubated for 30 min. Finally, the optical density was evaluated with a microplate reader at 490 nm.

Statistical analysis: design of experiment

To evaluate the effect of the composition on the final properties of the sponges we conducted a 2^3 full factorial design of experiment (DOE), 3 variables were studied: the fibroin – MA solution concentration, the percentage of surfactant, and the percentage of photoinitiator. For each variable we choose two levels (-1 and +1), listed in **table 1**, three samples were prepared for each of the 2^3 possible variables combinations, for a total of 24 samples. For each sample, we studied some properties of interest (yield) and we build a predictive model associating the composition variables to the properties. In **table 3** the general model is reported this model include all the first order factor that correlates the porosity directly to the composition variables, the second order factors that consider how a couple of variables mutually interacts with each other and a third order factor that was taken into account for the mutual interaction of all variables. Is worth to notice that "mixed" terms are not usually considered in methods that study the variation of one property vs. one variable. A Pareto plot and a half-normal plot was used to evaluate which terms to include in the model then an analysis of variance (ANOVA) test was then performed to evaluate their significance. The function of the considered yield (F(Y)) was chose in order to make the residuals normal distributed.

$F(Y) = c_1 * A + c_2 * B + c_3 * C + c_4 * A * B + c_5 * A * C + c_6 * B * C + c_7 * B * C + c_8 * A * B * C$		
	Levels	
Factor (Variable)	**-1**	**+1**
Fibroin - MA concentration [%]	10	20
Tween 20 [% w/w]	0	11
LAP [% w/w]	1	15

Table 3: Factors and their respective levels, considering a property Y a general model can be built to evaluate it as a function of the considered variables. This model not only includes a first order terms but also "mixed" terms that take into account the interaction between variables. Not all the terms are usually included into the model but only terms that are statistically relevant in accordance with the ANOVA test.

Results and discussion

Silk fibroin sponges were widely reported in literature as scaffolds for different tissues engineering applications: from bones to soft tissue. Different methods were used to fabricate this material and each of them gives a different distribution of the pore diameters. The porosity of a sponge and the possibility to tune it is extremely important to properly design a scaffold. The optimal pore size for tissue regeneration is dependent on the tissue to treat: a structure in which both macropores and micropores are present ensures both cell attachment and proliferation, and the neovascularization[58]. The prepared samples are shown in **figure 4**. Only the initial composition of the sponge was changed leaving the process parameters constant. Interestingly, just from a visual comparison, we can clearly see how the percentage of LAP influence the colour of the sponge. This is not related to the colour of LAP that results to be bright white in its solid form, and its water solution perfectly transparent. The colour could be, instead, related to crosslinking or to a reaction that occur by the presence of LAP, in fact it appears only after the UV treatment in sample with a high amount (15%) of LAP. The Sil-MA with low amount (1%) of LAP was subjected to the same UV treatment, for the same time and with the same power. The photoyellowing effect, in this case, did not occur, so the direct effect of the UV radiation on the protein can be excluded. The impact of the UV radiation on amino acids, as previously reported[59] is function of

time, energy adsorbed and wavelength. In particular, photoyellowing is mainly due to free radical photooxidation of the Triptofan and Tyrosine residues, leading to the formation of yellow products. In our case the irradiation was conducted with an LED centered at 365nm, a region in which the photo-yellowing has a little effect[59]. However, the oxidation of tyrosine and tryptophan residues could be probably triggered by the presence of LAP. A more detailed study of this phenomenon should be performed but is out of the scope of this work. Another noticeable difference, clearly visible in **figure 4**, is related to samples uniformity. In fact, sample made by the 20 % solution, regardless the other factors, shown a discontinuous structure with large holes. In addition, the higher degree of crosslinking ensures better performance in terms of stability in water, especially during the first hour (before the transition to the β structure, occurring due to the water treatment). The design of experiment method was performed to understand which of the components of the sponge composition are crucial to modify the studied properties. The porosity was analyzed by SEM imaging and with an automated method for pore recognition and area measurement. FTIR confirmed the successful functionalization and the fact that the composition does not influence the secondary structure. The dissolution test proved the influence of the percentage of photoinitiator and thus the level of crosslinking on the degradation of the sponge, especially after the first day of the test.

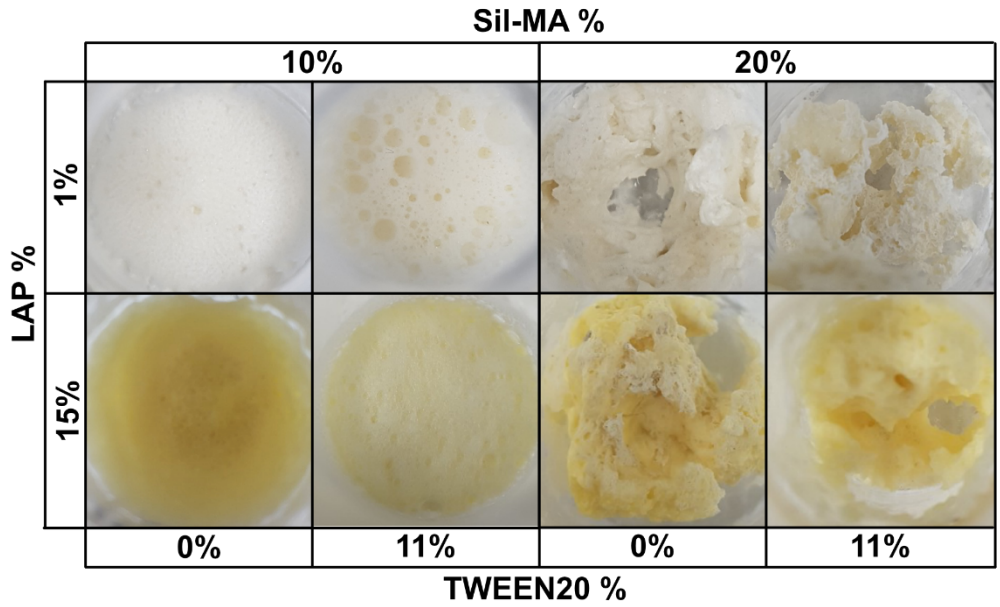

Figure 4: Prepared samples, for sake of clarity only 1 sample per condition is showed. The addition of 75mg of LAP makes the samples yellowish after the photo – crosslinking, this effect is present only on the skin of the sponges not inside. Samples prepared with a 10 % solution appears to be more uniform than the samples prepared with a 20 % solution, this can be attributed to a partial gelation during the process of the sample with higher concentration.

Structural Analysis

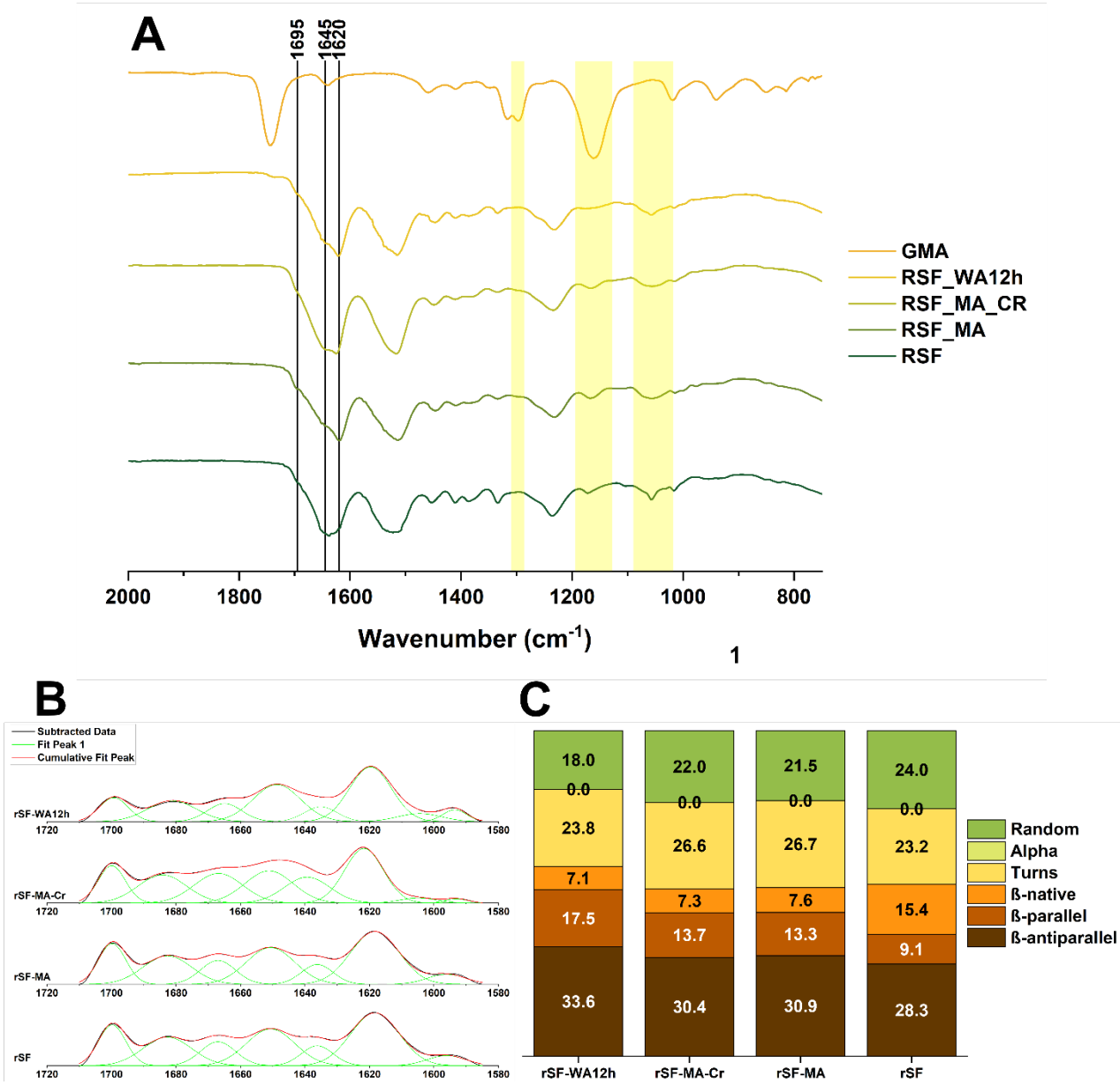

Figure 5: ***(A)*** *Comparison between the FTIR – ATR spectra of a regenerated fibroin(rSF), a methacrylate (rSF – MA) fibroin and a crosslinked methacrylated fibroin film (rSF_MA_Cr), a water annealed fibroin film (rSF_WA12h), and the glycidyl methacrylate in solution. Small variation the rSF-MA spectra due to the presence of the functional group could be recognized at 1265 (CHOH stretching), 1165 (CH_2 wagging stretching) and 1015 cm^{-1} (out of plane CH stretching) indicate the presence of the methacrylate functional group then the successful reaction between GMA and silk fibroin. In the primary amide peak, the increase in the intensity at 1695 and 1620 cm^{-1} (both associated with β – structures) and the decrease at 1645 cm^{-1} (random coil) indicates the change in the secondary structure of the fibroin to a more crystalline form after methacrylation, change that is maintained also after crosslinking.* ***(B)*** *Gaussian fitting of the Fourier self-deconvolution (FSD) conducted on the primary amide peaks to determine the percentage of the different secondary structure.* ***(C)*** *Comparison between the secondary structures of the regenerated and methacrylated silk fibroin films: an increase in the percentage of the β – antiparallel structure and in a minor amount of the turns and β – parallel structure and the contemporary decrease in the random coil and β – native structures, indicates the transition to a more stable configuration. This indicates that the presence of the*

functional group influences the secondary structure configuration of the protein. The secondary structure after crosslinking remain basically unchanged, only slightly variations can be detected. The comparison of the crosslinked Sil-MA (rSF-MA-Cr) with a 12 h water annealed protein (rSF-WA12h) revealed that the last one is inherently higher in parallel and antiparallel β structures and lower in Random structure.

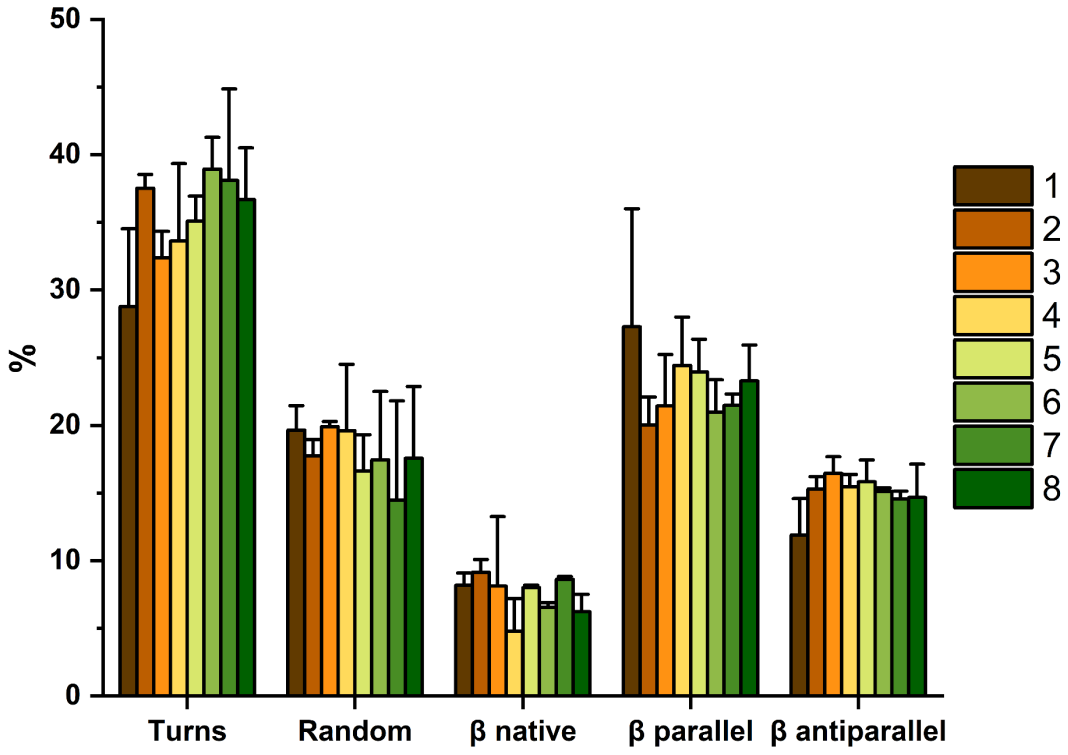

Figure 6: Secondary structure percentage composition of the 8 types of sponges, no statistical difference can be detected by ANOVA analysis between the single secondary structure components of the different compositions. From this analysis we can assert that the composition does not significantly affect the secondary structure.

Both the presence of functional groups and the protein secondary structure were studied by infrared spectroscopy (FTIR-ATR). In **figure 5A**, the comparison between modified (crosslinked and uncrosslinked), and regenerated (normal and water annealed for 12 h) silk fibroin films is shown. In addition, the spectra collected by a glycidyl methacrylate (GMA) solution is reported as reference. In accordance with previous works[32], small variation of the spectra due to the presence of the functional group can be individuated on the methacrylated silk fibroin films (both crosslinked and uncrosslinked)

in comparison with the unmodified (**figure 5A**). In particular the peaks at 1265 (CHOH stretching), 1165 (CH_2 wagging stretching) and 1015 cm^{-1}(out of plane CH stretching), indicate the presence of methacrylate functional groups and they can be recognized also in the GMA spectra. However, no variation could be detected between the crosslinked and uncrosslinked Sil-MA films. The chemical modification influenced the protein secondary structure as can be seen from **figure 5C** as a result of the deconvolution of the primary amide peak (**figure 5B**). A slight increase of the β parallel and antiparallel structures at the expense of a decrease of the amount of random coil and β native structures was detected after the methacrylation (**rSF_MA**) in comparison with the original protein (**rSF**). After the UV exposure instead, the secondary structure was almost unchanged (**rsf_MA_Cr**). An interesting result appears from the comparison of the secondary structures of the crosslinked methacrylated protein (**rSF_MA**) with a 12h water annealed fibroin (**rSF_WA12h**), the water annealing stabilize the protein by the formation of β parallel and antiparallel structures at the expense of the Random coil. In the comparison the water annealed protein resulted to be slightly more crystalline then the chemically crosslinked protein. The decrease in the β native and the increase in parallel and antiparallel β-structures has been recently recognized[42,60] as one of the main reason of the protein stabilization. We analyzed the secondary structure of each of the 3 replicates of sponges prepared with 8 compositions by the study of their primary amide peak, then an ANOVA test was performed to individuate if any significant difference in the amount of each single structure was present among the composition. The result of the deconvolution and peak fitting is shown in **figure S4**, the ANOVA tables (one for each specific secondary structure) are shown in **table S3-S7**. The data is presented in **figure 6** as histograms divided in groups accordingly with each secondary structure. For each secondary structure (group), there were no significant difference between their percentage amounts among the different compositions. This allows us to state that the sponge composition had no appreciable effect on the sponge secondary structure. As consequence it was not possible to build an empirical model using the DOE method.

Pore distribution and morphology

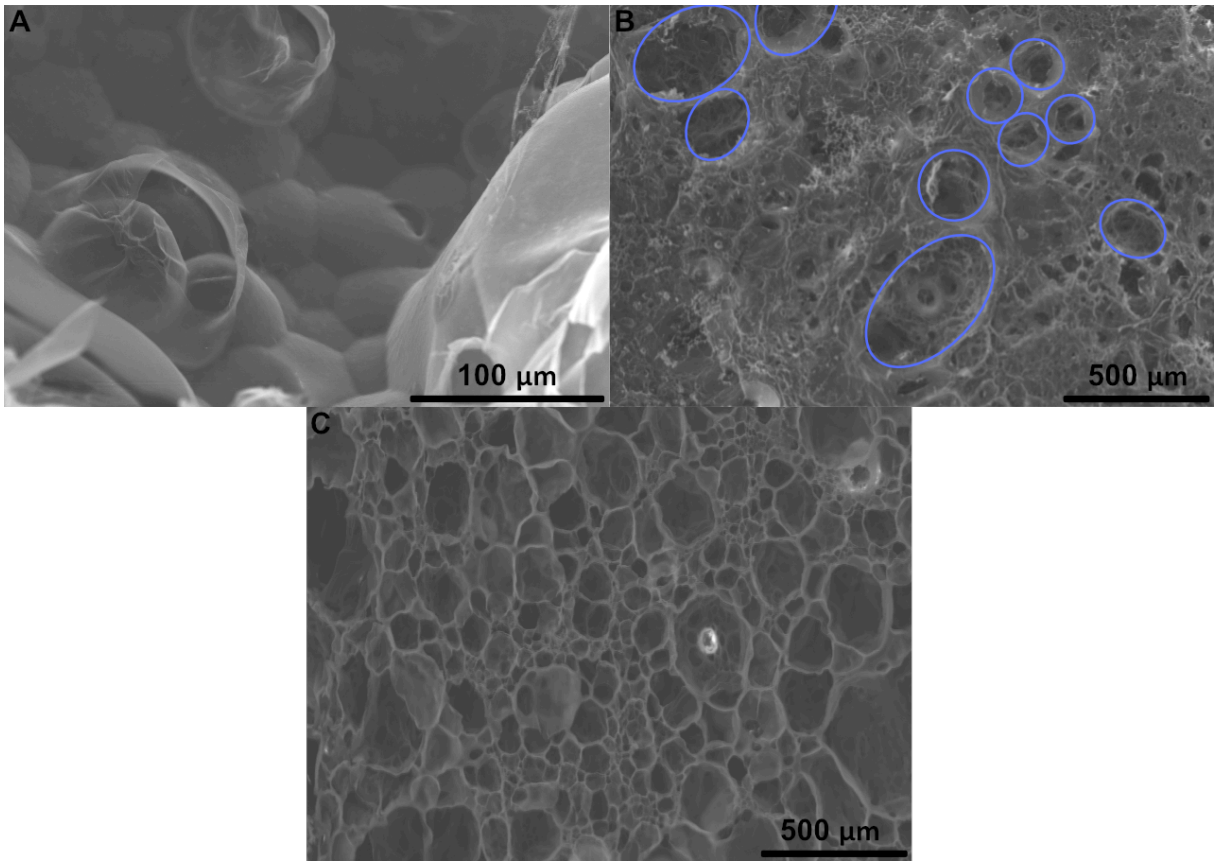

*Figure 7: SEM micrograph of the sponge. (**A**) the bubbles structure produced by the mixer is clearly visible in the background. Some cut bubbles are present in the first plane. From this image, we can deduce that we were able to effectively stabilize the microstructure by photocrosslinking. (**B**) A superficial image shows how from the larger pores is possible to note the underling pore structures indicating that the porosity is interconnected. (**C**) A micrography of the cross section shows a wide distribution of pores diameters.*

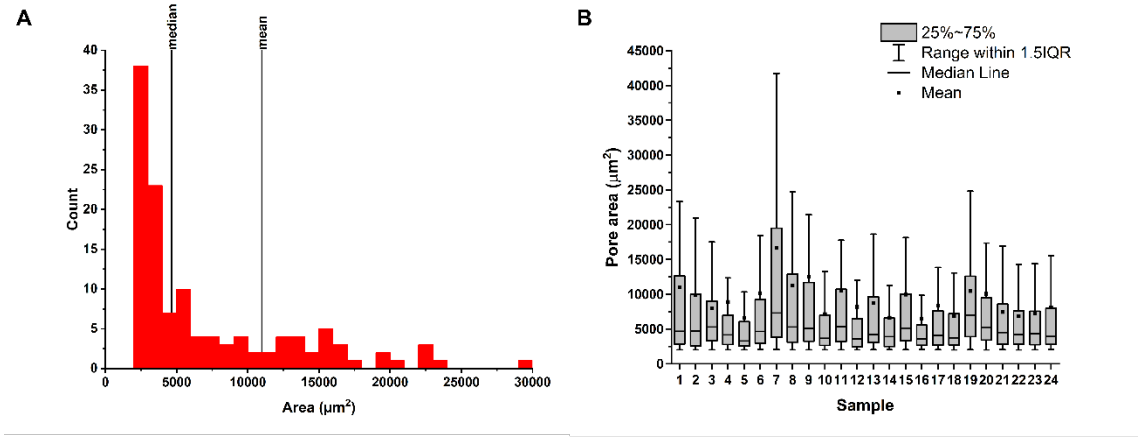

Figure 8: ***(A)*** *Pore distribution of the first sample (1A of figure 3). All distributions obtained from images were skewed, implying that the median and the mean are not in the same position, so both were considered as statistical measure of the porosity.* ***(B)*** *The box-cox plot of samples pore distributions shows that all of them were skewed: in fact, the mean (black square) is not in the same position as the median (black line). 50% of the data points are concentrated inside the interquartile range represented by the box (IQR, 25% - 75%) and the 80% inside the whiskers (90% - 10%).*

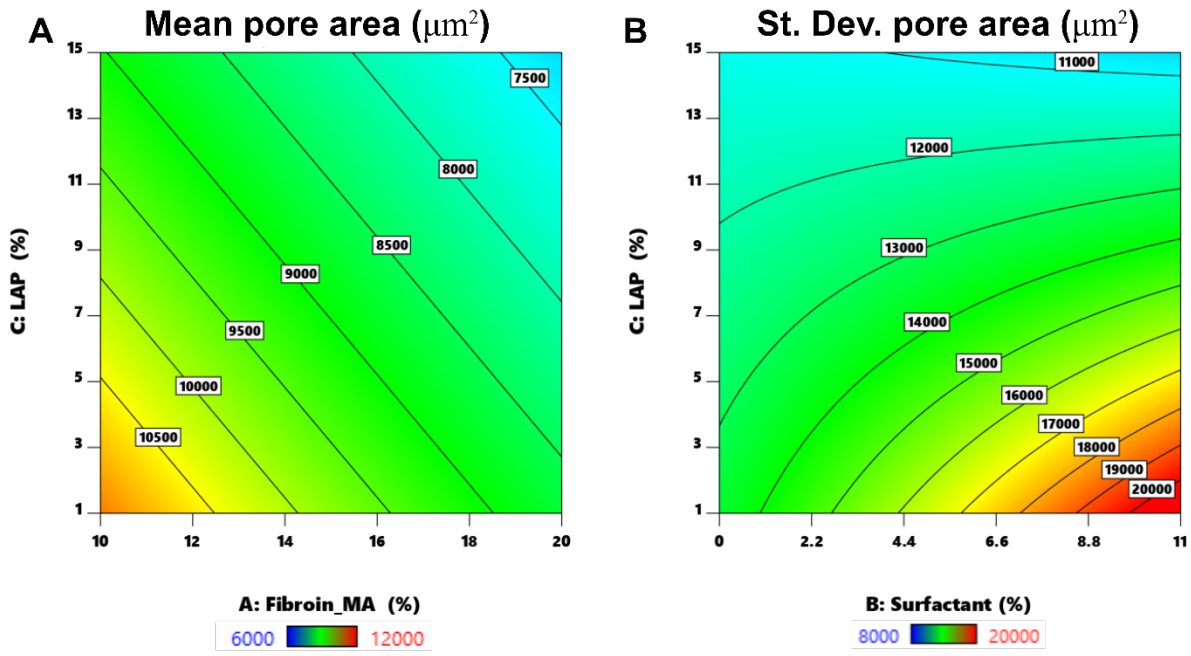

Figure 9: ***(A)*** *Modeled mean pore area trend (the scales are inverted for the sake of clarity). All the considered variables influenced the trend: the increasing of the surfactant volume and the decreasing of both the solution concentration and the initiator tend to increase the mean pore area.* ***(B)*** *Modeled standard deviation (St. Dev.), in this case the trend was not influenced by the protein concentration. The St. Dev. increase with an increase of the surfactant and a decreasing of an initiator.*

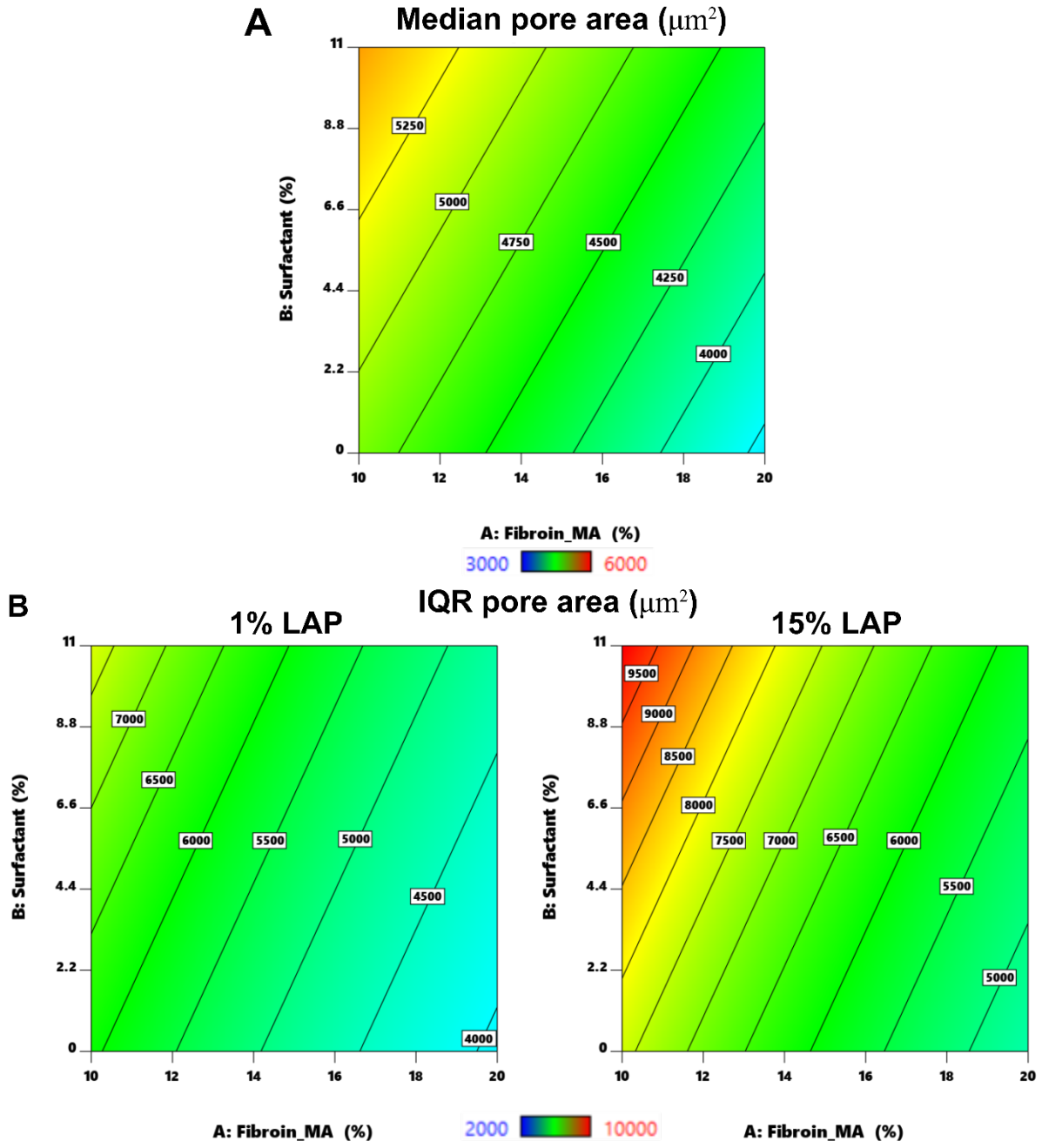

*Figure 10: **(A)** Modeled median pore area, in this case only the protein and the initiator concentration have an influence. An increasing of the area could be detected with an increase of both factors. **(B)** Modeled interquartile range (IQR) all the three factors influence the trend. The IQR increases with the decrease of the protein concentration, the increase of the surfactant and the decrease of the initiator.*

From the SEM micrograph of **figure 7A** we could observe how the initial structure was stabilized and, in fact, the original walls of the air bubble are clearly visible. The pores resulted to be interconnected how proved by the superficial micrograph visible in **figure 7B**. In fact, from the superficial pores the

underling pore structure is visible indicating that the pores are interconnected. This kind of structure gives a sort "spherical" interconnected pores visible in the micrographs of **figure 7B**, with a wide distribution. The distribution of the pore area was evaluated by the analysis of 2 images per each sample (**figure 7**). All the distribution resulted to be not normal and skewed to the left as shown in **figure 8A** and **B**, for this reason, we evaluated both the mean and the standard deviation, and the median and the interquartile range (IQR). The results are listed in **table S1** and **table S2**. Both the mean and the median were below 100 µm but considering the standard deviation and the interquartile range (IQR) we could deduce that a consistent part of distributions was above 100 µm. The third interquartile and the maximum pore diameter gives a measurement of how spread each distribution was: in all cases the first results to be higher than 79 µm and the second higher than 150 µm. We modeled, as statistical parameters the mean and the median pore area, the standard deviation and the interquartile range (IQR). All the models were significant (ANOVA tables from **table S3** to **table S6**). From the ANOVA table (**table S3**) we could assert that only two terms resulted to influence the mean, in order of importance: A – the concentration of the fibroin solution and C – the percentage of the photoinitiator (LAP). A decreasing of these terms results in an increase of the mean pore area (**figure 9A**). Unexpectedly the percentage of surfactant (term B) did not play a role in the mean pore area. Higher order terms resulted not significant, so the model could be considered linear. The standard deviation, as can be seen in its ANOVA table (**table S4**), is instead influenced by the percentage of the surfactant (term B) as well as the percentage of photoinitiator (term C): the increasing of the former and a decreasing of the latter ensured a higher standard deviation resulting in a broader distribution (**figure 9B**). The median pore area, from its ANOVA table (**table S5**) resulted to be influenced by A – the fibroin-MA concentration and B – the percentage of surfactant. A decreasing of the first term and an increase of the second gave an increment in the median pore area (**figure 10A**). The interquartile range was influenced by all the three considered factors (**table S6**): a

decreasing in A – the concentration of fibroin in solution, an increasing of B – the percentage of surfactant and C – the percentage of photoinitiator gave an increase in the IQR (**figure 10B**).

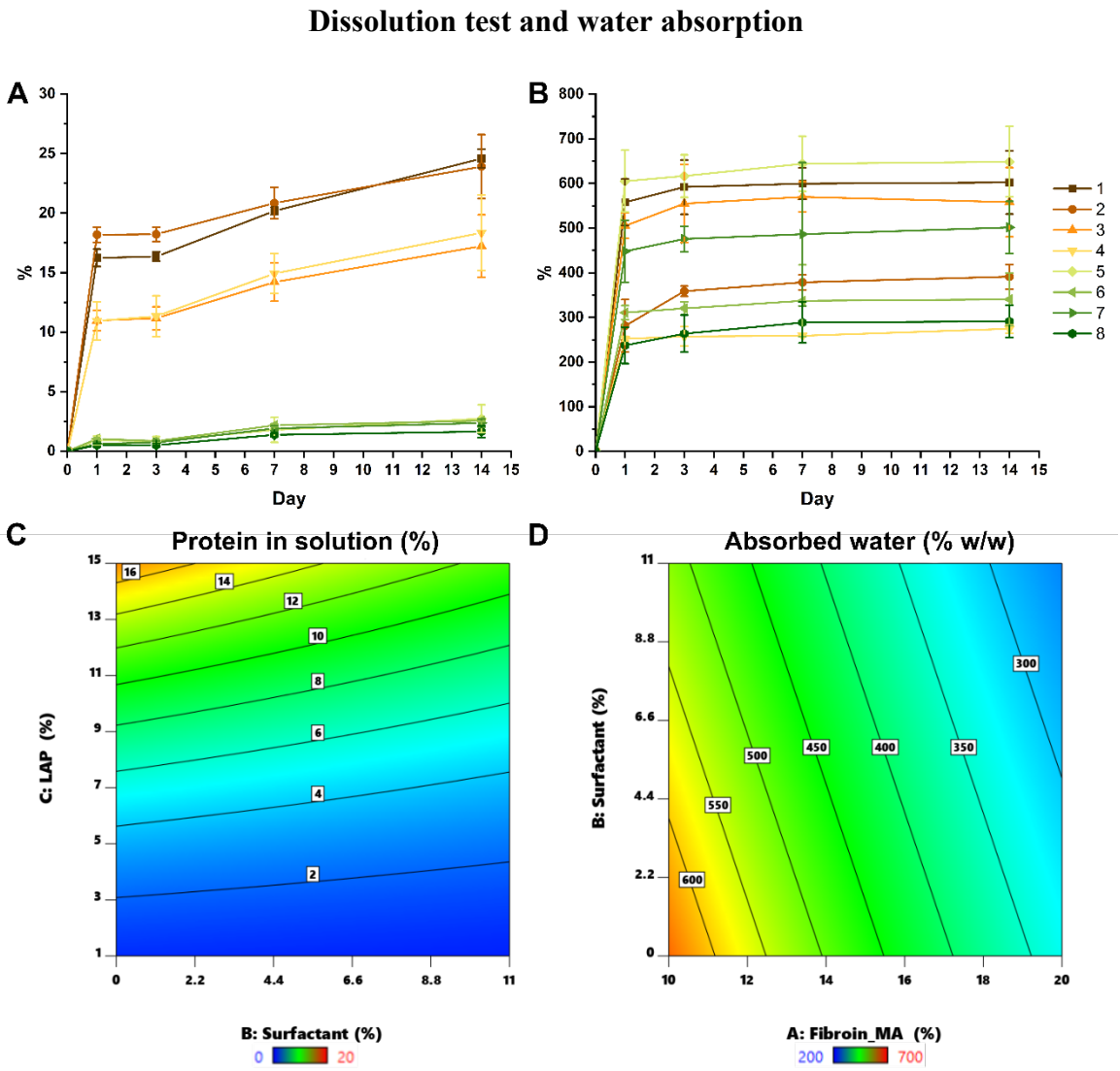

*Figure 11: **(A)** Dissolution test in simulated body fluid (SBF). A striking effect can be observed passing from 5 mg (samples 1-4) to 75 mg (samples 5-8) of photoinitiator, a second difference can be observed between the sample 1-2 and 3-4 and this is related to the presence of the surfactant. **(B)** Water absorption. In this case, a difference can be individuated between the samples 1-3-5-7 and the samples 2-4-6-8, this is due to the concentration of the initial solution that pass from 10 to 20%. **(C)** Modeled dissolution at day 3, the decrease of the percentage of surfactant and the percentage of photoinitiator increase the percentage of dissolved fibroin. **(E)** Modeled water absorption on day 3, the decrease of the protein concentration and percentage of surfactant increase the amount of adsorbed water.*

The dissolution in SBF and the water absorption are reported in **figure 11A** and **B** as a percentage of the initial weight of the sponge. The dissolution at day 1 is dramatically different for samples with different compositions, in particular we could recognize the effect of the percentage of photoinitiator (sample 1-4 versus samples 4-8) and, with a minor contribution, the effect of the percentage of the surfactant (sample 1-2 versus sample 3-4). These differences remain stable throughout the experimental time. These two parameters resulted to be significant also from an ANOVA analysis (**table S11**), and the model resulted to be linear because of the lack of higher order terms. The model (**figure 11C**) showed that a decrease in the percentage of surfactant and photoinitiator gives an increase in the amount of dissolved fibroin. The percentage of photoinitiator influences the degree of crosslinking and consequently the sponge stability. Thus, a lower percentage of LAP gives a higher amount of solubilized sponge. Instead, the lower percentage of the surfactant gives a lower dispersion of the pore distribution that could be related to the higher stability. The only clear effect visible from the water absorption is due to the protein concentration in solution (**figure 11B** sample 1, 3, 5, 7 versus sample 2, 4, 6, 8). Interestingly, the ANOVA table for the water absorption at day 3 (**table S12**) revealed a significant influence of parameters like the percentage of photoinitiator alone and in combination with the percentage of surfactant (B*C). The model is shown in **figure 11D**: the decrease of the protein concentration and of the percentage of surfactant increase the amount of adsorbed water. Since the median pore area goes in the same direction, we could assert that a decrease in the area of the pores (in the lower region of the dispersion) could result in a higher amount of adsorbed water. The data were model only for the day 3, because as stated before the effect of the composition on the dissolution and water absorption is visible from day 1; then even though there are small variations, the mutual differences between the data of different compositions remains constant throughout the duration of the experiment.

Compression test

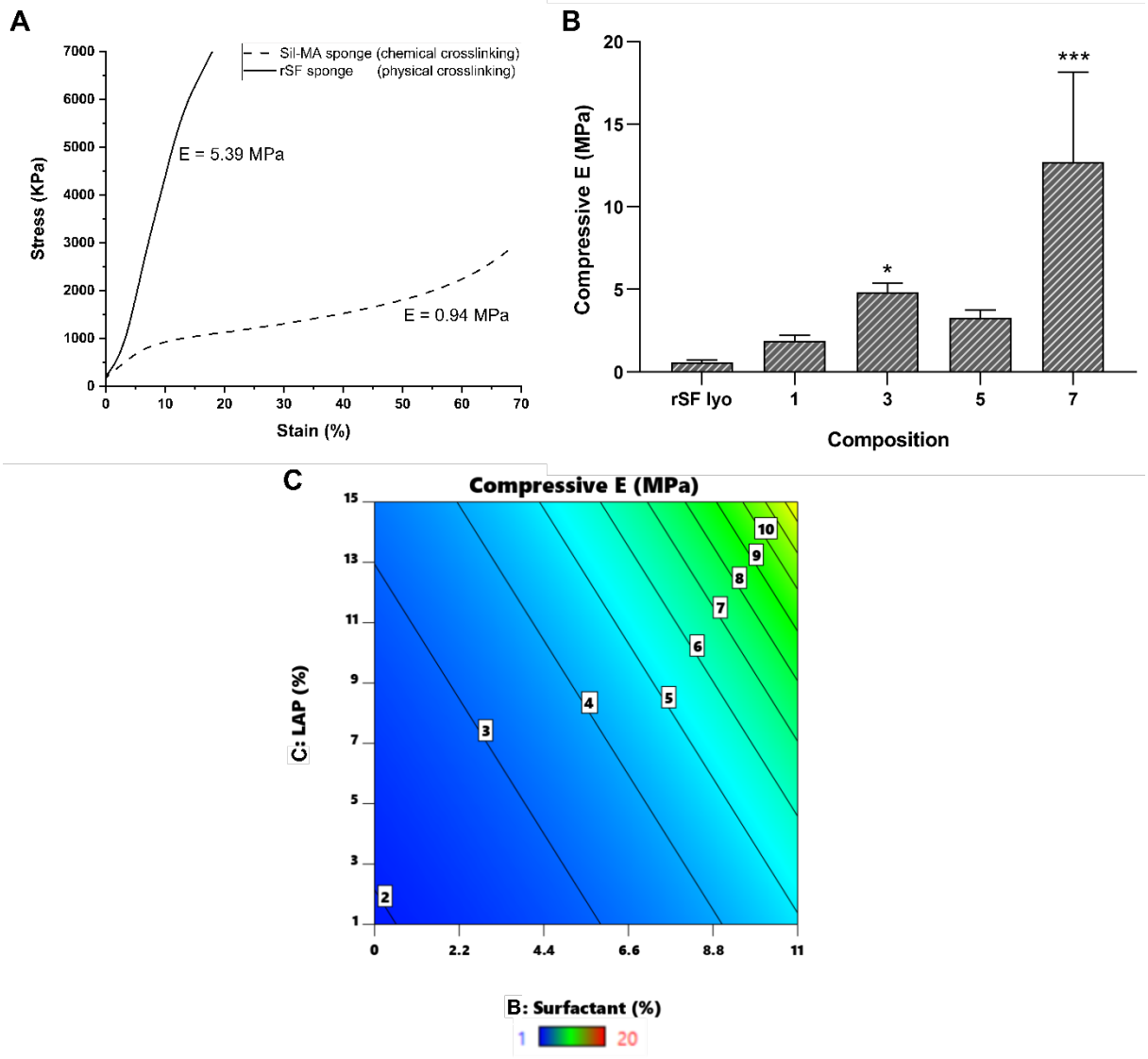

Figure 12: ***(A)*** *Stress-strain curve to compare a chemically crosslinked sil-MA sponge (composition 3) and a physically crosslinked lyophilized fibroin sponge. The compressive modulus of the chemical crosslinked sponge resulted to be 5 times higher than the compressive modulus of the physical crosslinked sponge.* ***(B)*** *Histogram reporting the mean (among 3 samples) and the standard deviation of different compositions, only the composition 3 and 7 resulted to be significantly different from the lyophilized sponge.* ***(C)*** *Surface plot of the empirical model for the compressive modulus both the increment of the percentage of surfactant and the percentage of photoinitiator increase the elastic compressive modulus.*

A compression test was performed only on samples made by a 10% Sil-Ma solution in comparison with a sponge made by the unmodified protein. Is worth noticing that we could not perform the test on the silk sponge obtained with the high concentrated solution (20%) in fact their structure as can be seen in **figure 1** was not suitable for a mechanical testing. However, we performed the test on samples with the

composition 1, 3, 5 and 7, taking as comparison a lyophilized silk fibroin sponge. As can be seen in **figure 12 A**, which reports a comparison between stress and strain curves of a crosslinked sponge (composition 3) and a lyophilized water annealed silk fibroin sponge, there is a striking difference between mechanical response and thus in the compressive young modulus. This difference can be attributed to the presence of chemical crosslink that ensured a compressive modulus five times higher than the physical crosslink (5.39 MPa versus 0.94 MPa). In **figure 12 B**, the mean and the standard deviation of different compositions is reported as histogram. From the ANOVA test (**table S14**) only the composition 3 and the composition 7 resulted to have a compressive modulus significantly different from the lyophilized, physically crosslinked, fibroin sponge. The model for the compressive modulus is reported in **figure 12 C**, both the increasing of the photoinitiator and the surfactant increase the mechanical strength. In this case the composition influenced the inverse square root of the compressive modulus (model in **table S18**).

Preliminary in vitro evaluation

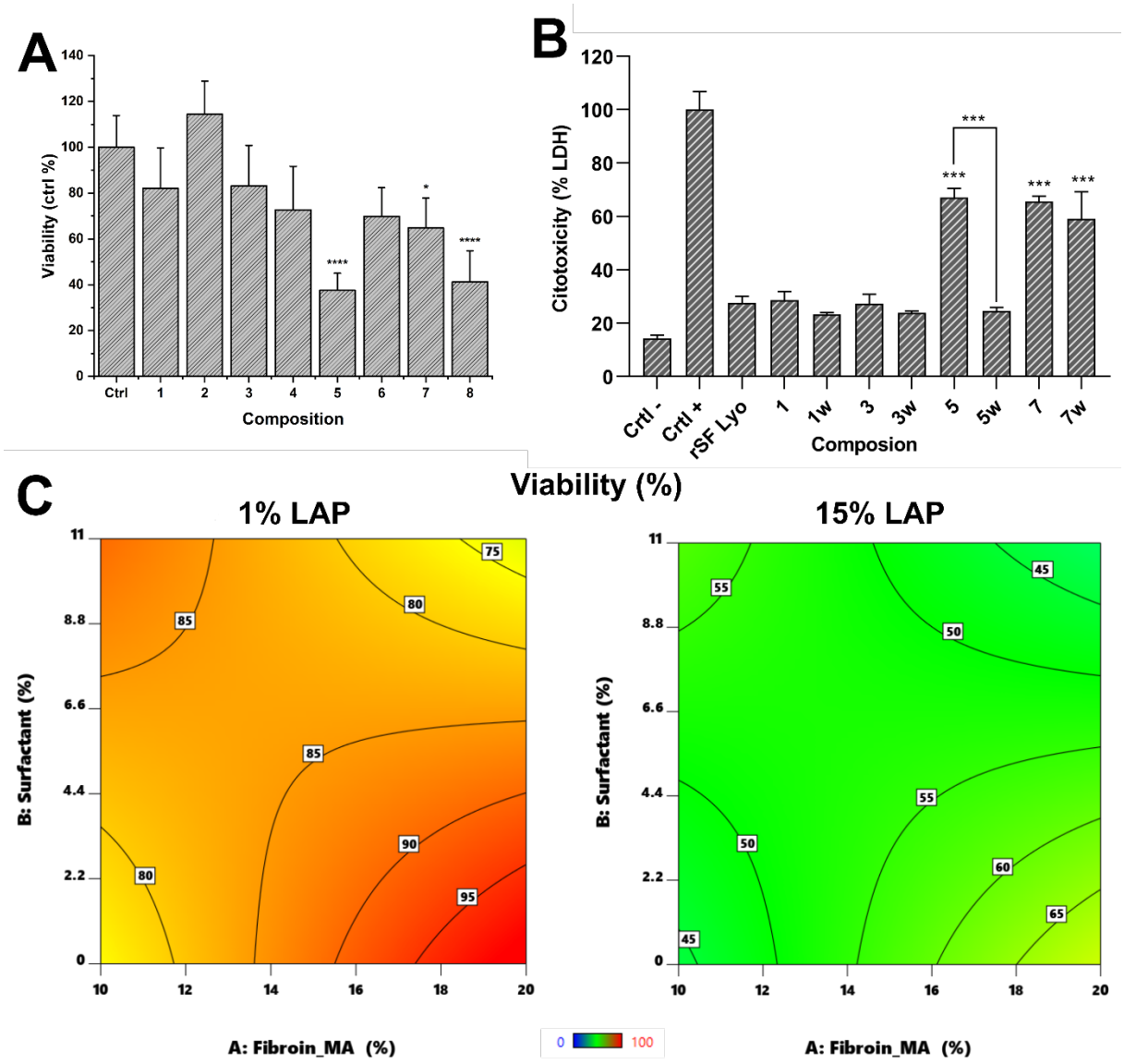

Figure 13: MTT assay response. ***(A)*** *The cell viability was evaluated as the percentage of the positive control, an ANOVA test was conducted to evaluate the significance versus the control: samples 5, and 8 results to have significantly lower viability. This effect is clearly due to the higher percentage of LAP as shown in figure* ***(C)*** *where the modeled response is shown. Passing from 1 to 15 % of LAP the model pass from around 95 to 65 % of cell viability in the best-case scenario. The response is not linear due to the significance of the term A*B - fibroin MA concentration * percentage of surfactant. The LDH assay on samples prepared with a 10% Sil-MA concentrated solution is shown in* ***(B)*** *it confirms the cytotoxicity of the photoinitiator in high concentration even in comparison with a sponge produced by the unmodified protein (compositions 5 and 7). However, a washing procedure can in some can mitigate the effect, decreasing the cytotoxicity (composition 7 versus 7w).*

The MTT assay was conducted to evaluate the cytocompatibility of the sponge and the cell viability: in **figure 13A** the percentage cell viability was reported for the different concentration of the sponge

prepared. The obtained results clearly infer that the increasing the initiator (LAP) concentration in the samples has an effect on decreasing the cell viability. The samples with lower initiator concentration (sample 1, 2, 3 and 4) are highly cytocompatible with cell viability around of 80 % and above. From these results, samples 1 to 4 are cytocompatible with the cell viability of 80% and above showing LAP 5 mg concentration in the sponge can be taken further for the *in vivo* studies before experimenting in larger animals. The ANOVA test (**table S15**) conducted against the control shown that a significant difference is present for the sample 5, and 8. This is related to the effect of the initiator, that, even though it is widely used in material with biological application[32,61–63], in high concentration could result toxic[64]. This became clear by using the collected data in combination with the DOE method. In fact, from the ANOVA table the main effect on the cell viability is due to the factor C – the percentage of photoinitiator. Unexpectedly, the second order mixed term fibroin-MA concentration * percentage of surfactant (A*B) resulted to be significant, so also the single terms A and B were included to maintain the model hierarchy. The effect of A*B is clearly visible in the curvature present in the model (**figure 13C**): A*B is negative, so, even if the concentration of protein is not relevant, due to this mixed term the viability is maximized at higher protein concentration and lower percentage of surfactant. Another maximum but with a lower viability is obtained when the surfactant is in its high level and the concentration of silk at its low level. The response surface undergoes a negative translation when the LAP quantity increases from 5 to 75 mg, confirming the cytotoxicity of LAP residues when used in high concentration. To further understand the effect of the photoinitiator residues we decided to evaluate the cytotoxic effect by a quantification of LDH released by cells during 48 h of incubation with the conditioned medium. The analysis was conducted only on samples made by a 10% concentrated Sil-MA solution (the samples with a structural coherency as can been seen in **Figure 1**). In this experiment, an additional comparison between sponges with and without a day of washing in water was added as reference a sponge made by lyophilization from the unmodified silk fibroin solution. In general, from **figure 13B** the values of not washed samples are

slightly higher than washed samples. In fact, the washing step after sponges' fabrication should remove the toxic residual of photoinitiator that can cause toxic effect on cells. Actually, except for sample 5, the washing step seems to not be so relevant for the cytotoxicity effect of the other samples. Sample 7 appears to be cytotoxic in both cases. Sample 1 and sample 2 can be compared to the reference sample (rSF lyo), which is not corresponding to a cytotoxic value.

Discussion

Sponge properties resulted to be composition dependent. In case of Sil-MA, the porosity and the compressive modulus on hydrogel were studied and resulted to be influenced by the concentration of protein in solution and the amount of GMA used in the modification reaction[32]. In our study, we confirmed the dependence of the mean pore area on the concentration of protein in solution, but we also proved its dependence on the percentage of photoinitiator (LAP). We studied the standard deviation as statistical parameter of the range of the mean pore area distribution. This parameter resulted to be influenced by the percentage of surfactant (Tween20) and LAP. The surfactant effect could be explained by considering the amphiphilic nature of its molecules, that allows an effective stabilization of the air-liquid interface[65–68] and, possibly, the formation of bigger bubbles. An increase in the percentage of LAP decreased the standard deviation. This could be related to the higher number of radicals produced thus the faster crosslinking[69] and the impossibility for the structure to partially collapse leaving bigger holes. The stability of the sponge in simulated body fluid was mainly influenced by the photoinitiator concentration that, influencing the degree of crosslinking[70], could modulates the mechanical and chemical stability. The effect surfactant amount was also significant; in this case the wider distribution of pore area due to an increase in the percentage of Tween 20 could probably explain the lower stability of the sponge due to the higher permeability to the solution[71,72]. The compressive young modulus increased as result of the chemical crosslinking, in this case our sponge resulted to be comparable with

results obtained with other methods as the dissolution of degummed fibroin in NaOH followed by lyophilization[73], a combination of salt-leaching and freeze drying[12], the addition of water soluble solvents (DMSO, ethanol, methanol) in low concentration to a high concentrated silk fibroin solution[17], the reinforcement of the fibroin scaffold with fibroin particles[74–76] or fibers[77–79]. In the preliminary *in vitro* test, the cell viability was primarily dependent on the percentage of photoinitiator. Even if this photoinitiator has been widely used for scaffold fabrication[32,61,70,80,81] it resulted to be, in our experiment, cytotoxic if used in high concentration. This discrepancy is probably due to the low concentration generally adopted in literature[32,61,70,80,81] (between 0.1 and 1 %), much lower than the concentration used in the high level of our experiment (15 %). The cell viability resulted to be influenced also by a second order mixed term, the surfactant volume and the percentage of photoinitiator resulted to be interacting factors. Considering that the absence of cytotoxicity is a prerequisite for a scaffold, the percentage of photoinitiator is the limiting factor of our protocol. However, an additional washing step resulted to be effective in eliminating the photoinitiator residue thus increasing and consequently decreasing the material cytotoxicity. The range of tunability of material properties could be in future expanded by considering other parameters in the experimental design (for instance, the energy absorbed from the sample during the UV exposure, usually tuned by tuning the time of the exposure).

Conclusions

Silk fibroin sponges are a widely studied material used as a scaffold in both for bones and for soft tissue engineering applications. Among their properties, porosity, mechanical and chemical stability are the most important ones. An open porosity with a wide distribution of diameters ensures an optimal cells attachment and growth while the stability in a simulated body fluid allows enough time to regenerate the tissue prior to the scaffold degradation. Both properties should be tunable to fit the requirement of the natural tissue. In this work, we were able to optimize a methodology to obtain a sponge from a

methacrylated fibroin (fibroin-MA) solution with tunable porosity and stability. The stability was ensured by the formation of a crosslinked network by exposure to UV light. This type of crosslinking can be defined as chemical, in contrast with the physical crosslinking in which the stability is ensured by a change in the protein conformation to the more stable beta structures. The infrared spectroscopy revealed the successful functionalization of the protein in which methacrylic groups were added by chemical reaction. The effect of the sponge composition on the secondary structure, the porosity distribution, the water absorption, the stability in SBF, and the cell viability was studied by a full factorial design of experiment (DOE). Using this method, we were able to model the significant parameters for each property of interest. This allow to change the properties just by changing the sponge composition. The secondary structure has been revealed not sensitive to a compositional change. The porosity distribution was proved to be dependent on several factors. In particular, the mean pore area increases when the concentration of the silk fibroin solution and the percentage of initiator (LAP) decrease. The increased percentage of added surfactant instead had no effect on the mean pore area but influences the standard deviation, increasing it. The same effect on the standard deviation was recorded when the percentage of LAP decrease. The sponge stability in SBF was strongly dependent on the percentage of photoinitiator (thus to the level of crosslinking) and in a smaller amount on the percentage of the surfactant. The water absorption resulted to increase with the decreasing of the surfactant and the LAP, in this case interestingly a second order term results to be significant: the term percentage of surfactant * percentage of LAP. The major impact of the cell viability is due to the percentage of photoinitiator that resulted to be cytotoxic in high concentration, also in this case, the second order term percentage of surfactant * percentage of LAP resulted to be significant giving a curvature in the model. In conclusion, we proved the flexibility of the studied method, and how the composition can be changed to tune the sponge properties. This method could be used to adapt the sponge properties to the application in particular in tissue engineering were stability, porosity and cell viability are critical issues.

Acknowledgment

The project leading to this application has received funding from the European Union's Horizon 2020 Research and Innovation Staff Exchange programme (RISE) under the Marie Skłodowska-Curie grant agreement MSCA-RISE 778078 (REMIX project).

References

(1) Kundu, B.; Rajkhowa, R.; Kundu, S. C.; Wang, X. Silk Fibroin Biomaterials for Tissue Regenerations. *Adv. Drug Deliv. Rev.* **2013**, *65* (4), 457–470. https://doi.org/10.1016/j.addr.2012.09.043.

(2) Holland, C.; Numata, K.; Rnjak-Kovacina, J.; Seib, F. P. The Biomedical Use of Silk: Past, Present, Future. *Advanced Healthcare Materials*. 2019. https://doi.org/10.1002/adhm.201800465.

(3) Kundu, S. C.; Dash, B. C.; Dash, R.; Kaplan, D. L. Natural Protective Glue Protein, Sericin Bioengineered by Silkworms: Potential for Biomedical and Biotechnological Applications. *Prog. Polym. Sci.* **2008**, *33* (10), 998–1012. https://doi.org/10.1016/j.progpolymsci.2008.08.002.

(4) Vepari, C.; Kaplan, D. L. Silk as a Biomaterial. *Prog. Polym. Sci.* **2007**, *32* (8–9), 991–1007. https://doi.org/10.1016/j.progpolymsci.2007.05.013.

(5) Karageorgiou, V.; Kaplan, D. Porosity of 3D Biomaterial Scaffolds and Osteogenesis.

Biomaterials. 2005. https://doi.org/10.1016/j.biomaterials.2005.02.002.

(6) Hutmacher, D. W. Scaffolds in Tissue Engineering Bone and Cartilage. In *The Biomaterials: Silver Jubilee Compendium*; 2006. https://doi.org/10.1016/B978-008045154-1.50021-6.

(7) Chen, G.; Ushida, T.; Tateishi, T. Scaffold Design for Tissue Engineering. *Macromolecular Bioscience*. 2002. https://doi.org/10.1002/1616-5195(20020201)2:2<67::AID-MABI67>3.0.CO;2-F.

(8) Hollister, S. J. Porous Scaffold Design for Tissue Engineering. *Nat. Mater.* **2005**, *4* (7), 518–524. https://doi.org/10.1038/nmat1421.

(9) Liao, C. J.; Chen, C. F.; Chen, J. H.; Chiang, S. F.; Lin, Y. J.; Chang, K. Y. Fabrication of Porous Biodegradable Polymer Scaffolds Using a Solvent Merging/Particulate Leaching Method. *J. Biomed. Mater. Res.* **2002**. https://doi.org/10.1002/jbm.10030.

(10) Yao, D.; Dong, S.; Lu, Q.; Hu, X.; Kaplan, D. L.; Zhang, B.; Zhu, H. Salt-Leached Silk Scaffolds with Tunable Mechanical Properties. *Biomacromolecules* **2012**. https://doi.org/10.1021/bm301197h.

(11) Zhang, X.; Cao, C.; Ma, X.; Li, Y. Optimization of Macroporous 3-D Silk Fibroin Scaffolds by Salt-Leaching Procedure in Organic Solvent-Free Conditions. *J. Mater. Sci. Mater. Med.* **2012**. https://doi.org/10.1007/s10856-011-4476-3.

(12) Yan, L. P.; Oliveira, J. M.; Oliveira, A. L.; Caridade, S. G.; Mano, J. F.; Reis, R. L. Macro/Microporous Silk Fibroin Scaffolds with Potential for Articular Cartilage and Meniscus Tissue Engineering Applications. *Acta Biomater.* **2012**. https://doi.org/10.1016/j.actbio.2011.09.037.

(13) Rnjak-Kovacina, J.; Wray, L. S.; Burke, K. A.; Torregrosa, T.; Golinski, J. M.; Huang, W.; Kaplan, D. L. Lyophilized Silk Sponges: A Versatile Biomaterial Platform for Soft Tissue Engineering. *ACS Biomater. Sci. Eng.* **2015**. https://doi.org/10.1021/ab500149p.

(14) Pei, Y.; Liu, X.; Liu, S.; Lu, Q.; Liu, J.; Kaplan, D. L.; Zhu, H. A Mild Process to Design Silk Scaffolds with Reduced β-Sheet Structure and Various Topographies at the Nanometer Scale. *Acta Biomater.* **2015**. https://doi.org/10.1016/j.actbio.2014.11.016.

(15) Bai, S.; Han, H.; Huang, X.; Xu, W.; Kaplan, D. L.; Zhu, H.; Lu, Q. Silk Scaffolds with Tunable Mechanical Capability for Cell Differentiation. *Acta Biomater.* **2015**. https://doi.org/10.1016/j.actbio.2015.04.004.

(16) Mandal, B. B.; Kundu, S. C. Non-Bioengineered Silk Fibroin Protein 3D Scaffolds for Potential Biotechnological and Tissue Engineering Applications. *Macromol. Biosci.* **2008**. https://doi.org/10.1002/mabi.200800113.

(17) Tamada, Y. New Process to Form a Silk Fibroin Porous 3-D Structure. *Biomacromolecules* **2005**, *6* (6), 3100–3106. https://doi.org/10.1021/bm050431f.

(18) Nam, Y. S.; Yoon, J. J.; Park, T. G. A Novel Fabrication Method of Macroporous Biodegradable Polymer Scaffolds Using Gas Foaming Salt as a Porogen Additive. *J. Biomed. Mater. Res.* **2000**. https://doi.org/10.1002/(SICI)1097-4636(2000)53:1<1::AID-JBM1>3.0.CO;2-R.

(19) Yao, D.; Liu, H.; Fan, Y. Fabrication of Water-Stable Silk Fibroin Scaffolds through Self-Assembly of Proteins. *RSC Adv.* **2016**. https://doi.org/10.1039/c6ra10670f.

(20) Maniglio, D.; Bonani, W.; Migliaresi, C.; Motta, A. Silk Fibroin Porous Scaffolds by N2O Foaming. *J. Biomater. Sci. Polym. Ed.* **2018**. https://doi.org/10.1080/09205063.2018.1423811.

(21) Whittaker, J. L.; Choudhury, N. R.; Dutta, N. K.; Zannettino, A. Facile and Rapid Ruthenium Mediated Photo-Crosslinking of Bombyx Mori Silk Fibroin. *J. Mater. Chem. B* **2014**, *2* (37), 6259–6270. https://doi.org/10.1039/c4tb00698d.

(22) Applegate, M. B.; Partlow, B. P.; Coburn, J.; Marelli, B.; Pirie, C.; Pineda, R.; Kaplan, D. L.; Omenetto, F. G. Photocrosslinking of Silk Fibroin Using Riboflavin for Ocular Prostheses. *Adv. Mater.* **2016**, *28* (12), n/a-n/a. https://doi.org/10.1002/adma.201504527.

(23) Su, D.; Yao, M.; Liu, J.; Zhong, Y.; Chen, X.; Shao, Z. Enhancing Mechanical Properties of Silk Fibroin Hydrogel through Restricting the Growth of β-Sheet Domains. *ACS Appl. Mater. Interfaces* **2017**. https://doi.org/10.1021/acsami.7b04623.

(24) Partlow, B. P.; Hanna, C. W.; Rnjak-Kovacina, J.; Moreau, J. E.; Applegate, M. B.; Burke, K. A.; Marelli, B.; Mitropoulos, A. N.; Omenetto, F. G.; Kaplan, D. L. Highly Tunable Elastomeric Silk Biomaterials. *Adv. Funct. Mater.* **2014**. https://doi.org/10.1002/adfm.201400526.

(25) Ribeiro, V. P.; da Silva Morais, A.; Maia, F. R.; Canadas, R. F.; Costa, J. B.; Oliveira, A. L.; Oliveira, J. M.; Reis, R. L. Combinatory Approach for Developing Silk Fibroin Scaffolds for Cartilage Regeneration. *Acta Biomater.* **2018**. https://doi.org/10.1016/j.actbio.2018.03.047.

(26) Zhou, B.; Wang, P.; Cui, L.; Yu, Y.; Deng, C.; Wang, Q.; Fan, X. Self-Crosslinking of Silk Fibroin Using H2O2-Horseradish Peroxidase System and the Characteristics of the Resulting Fibroin Membranes. *Appl. Biochem. Biotechnol.* **2017**. https://doi.org/10.1007/s12010-017-2417-4.

(27) Kurland, N. E.; Dey, T.; Kundu, S. C.; Yadavalli, V. K. Precise Patterning of Silk Microstructures Using Photolithography. *Adv. Mater.* **2013**, *25* (43), 6207–6212. https://doi.org/10.1002/adma.201302823.

(28) Liu, W.; Zhou, Z.; Zhang, S.; Shi, Z.; Tabarini, J.; Lee, W.; Zhang, Y.; Gilbert Corder, S. N.; Li, X.; Dong, F.; et al. Precise Protein Photolithography (P3): High Performance Biopatterning Using Silk Fibroin Light Chain as the Resist. *Adv. Sci.* **2017**, *1700191* (9). https://doi.org/10.1002/advs.201700191.

(29) Bucciarelli, A.; Pal, R. K.; Maniglio, D.; Quaranta, A.; Mulloni, V.; Motta, A.; Yadavalli, V. K.; Bucciarelli, A.; Maniglio, D.; Quaranta, A.; et al. Fabrication of Nanoscale Patternable Films of Silk Fibroin Using Benign Solvents. **2017**, *201700110*, 1–9. https://doi.org/10.1002/mame.201700110.

(30) Bucciarelli, A.; Mulloni, V.; Maniglio, D.; Pal, R. K.; Yadavalli, V. K.; Motta, A.; Quaranta, A. A Comparative Study of the Refractive Index of Silk Protein Thin Films towards Biomaterial Based Optical Devices. *Opt. Mater. (Amst).* **2018**, *78*, 407–414. https://doi.org/10.1016/j.optmat.2018.02.058.

(31) Furuzono, T.; Ishihara, K.; Nakabayashi, N.; Tamada, Y. Chemical Modification of Silk Fibroin with 2-Methacryloyloxyethyl Phosphorylcholine. II. Graft-Polymerization onto Fabric through 2-Methacryloyloxyethyl Isocyanate and Interaction between Fabric and Platelets. *Biomaterials* **2000**, *21* (4), 327–333. https://doi.org/10.1016/S0142-9612(99)00177-5.

(32) Kim, S. H.; Yeon, Y. K.; Lee, J. M.; Chao, J. R.; Lee, Y. J.; Seo, Y. B.; Sultan, M. T.; Lee, O. J.; Lee, J. S.; Yoon, S. Il; et al. Precisely Printable and Biocompatible Silk Fibroin Bioink for Digital Light Processing 3D Printing. *Nat. Commun.* **2018**, *9* (1), 1–14. https://doi.org/10.1038/s41467-018-03759-y.

(33) Montgomery, D. C. *Design and Analysis of Experiments Eighth Edition*; 2012. https://doi.org/10.1198/tech.2006.s372.

(34) Rockwood, D. N.; Preda, R. C.; Yücel, T.; Wang, X.; Lovett, M. L.; Kaplan, D. L. Materials Fabrication from Bombyx Mori Silk Fibroin. *Nat. Protoc.* **2011**, *6* (10), 1612–1631. https://doi.org/10.1038/nprot.2011.379.

(35) Saeb, M. R.; Bakhshandeh, E.; Khonakdar, H. A.; Mäder, E.; Scheffler, C.; Heinrich, G. Cure Kinetics of Epoxy Nanocomposites Affected by MWCNTs Functionalization: A Review. *Sci. World J.* **2013**. https://doi.org/10.1155/2013/703708.

(36) Maziz, A.; Leprette, O.; Boyer, L.; Blatché, C.; Bergaud, C. Tuning the Properties of Silk Fibroin Biomaterial via Chemical Cross-Linking. *Biomed. Phys. Eng. Express* **2018**. https://doi.org/10.1088/2057-1976/aae3b2.

(37) Fairbanks, B. D.; Schwartz, M. P.; Bowman, C. N.; Anseth, K. S. Photoinitiated Polymerization

of PEG-Diacrylate with Lithium Phenyl-2,4,6-Trimethylbenzoylphosphinate: Polymerization Rate and Cytocompatibility. *Biomaterials* **2009**, *30* (35), 6702–6707. https://doi.org/10.1016/j.biomaterials.2009.08.055.

(38) Hu, X.; Kaplan, D.; Cebe, P. Determining Beta-Sheet Crystallinity in Fibrous Proteins by Thermal Analysis and Infrared Spectroscopy. *Macromolecules* **2006**, *39* (18), 6161–6170. https://doi.org/10.1021/ma0610109.

(39) Jung, C. Insight into Protein Structure and Protein-Ligand Recognition by Fourier Transform Infrared Spectroscopy. *Journal of Molecular Recognition*. 2000. https://doi.org/10.1002/1099-1352(200011/12)13:6<325::AID-JMR507>3.0.CO;2-C.

(40) Mouro, C.; Jung, C.; Bondon, A.; Simonneaux, G. Comparative Fourier Transform Infrared Studies of the Secondary Structure and the CO Heme Ligand Environment in Cytochrome P-450cam and Cytochrome P-420cam. *Biochemistry* **1997**. https://doi.org/10.1021/bi9700173.

(41) Teramoto, H.; Miyazawa, M. Molecular Orientation Behavior of Silk Sericin Film as Revealed by ATR Infrared Spectroscopy. *Biomacromolecules* **2005**. https://doi.org/10.1021/bm0500547.

(42) Shimanovich, U.; Ruggeri, F. S.; De Genst, E.; Adamcik, J.; Barros, T. P.; Porter, D.; Müller, T.; Mezzenga, R.; Dobson, C. M.; Vollrath, F.; et al. Silk Micrococoons for Protein Stabilisation and Molecular Encapsulation. *Nat. Commun.* **2017**, *8* (May), 1–9. https://doi.org/10.1038/ncomms15902.

(43) Shivu, B.; Seshadri, S.; Li, J.; Oberg, K. A.; Uversky, V. N.; Fink, A. L. Distinct β-Sheet Structure in Protein Aggregates Determined by ATR-FTIR Spectroscopy. *Biochemistry* **2013**. https://doi.org/10.1021/bi400625v.

(44) Ruggeri, F. S.; Longo, G.; Faggiano, S.; Lipiec, E.; Pastore, A.; Dietler, G. Infrared Nanospectroscopy Characterization of Oligomeric and Fibrillar Aggregates during Amyloid Formation. *Nat. Commun.* **2015**. https://doi.org/10.1038/ncomms8831.

(45) Zandomeneghi, G.; Krebs, M. R. H.; McCammon, M. G.; Fändrich, M. FTIR Reveals Structural Differences between Native β-Sheet Proteins and Amyloid Fibrils. *Protein Sci.* **2009**, *13* (12), 3314–3321. https://doi.org/10.1110/ps.041024904.

(46) Tretinnikov, O. N.; Tamada, Y. Influence of Casting Temperature on the Near-Surface Structure and Wettability of Cast Silk Fibroin Films. *Langmuir* **2001**. https://doi.org/10.1021/la010791y.

(47) Taddei, P.; Monti, P. Vibrational Infrared Conformational Studies of Model Peptides Representing the Semicrystalline Domains of Bombyx Mori Silk Fibroin. *Biopolymers* **2005**. https://doi.org/10.1002/bip.20275.

(48) GOORMAGHTIGH, E.; CABIAUX, V.; RUYSSCHAERT, J. -M. Secondary Structure and Dosage of Soluble and Membrane Proteins by Attenuated Total Reflection Fourier-transform Infrared Spectroscopy on Hydrated Films. *Eur. J. Biochem.* **1990**. https://doi.org/10.1111/j.1432-1033.1990.tb19354.x.

(49) Dong, A.; Huang, P.; Caughey, W. S. Protein Secondary Structures in Water from Second-Derivative Amide I Infrared Spectra. *Biochemistry* **1990**. https://doi.org/10.1021/bi00465a022.

(50) Monti, P.; Freddi, G. Raman Spectroscopic Studies of Silk Fibroin from Bombyx Mori. *J. Raman Spectrosc.* **1998**, *29* (January), 297–304. https://doi.org/10.1002/(SICI)1097-4555(199804)29:4<297::AID-JRS240>3.0.CO;2-G.

(51) Wilson, D.; Valluzzi, R.; Kaplan, D. Conformational Transitions Model Silk Peptides. *Biophys. J.* **2000**. https://doi.org/10.1016/S0006-3495(00)76813-5.

(52) Chen, X.; Shao, Z.; Marinkovic, N. S.; Miller, L. M.; Zhou, P.; Chance, M. R. Conformation Transition Kinetics of Regenerated Bombyx Mori Silk Fibroin Membrane Monitored by Time-Resolved FTIR Spectroscopy. *Biophys. Chem.* **2001**, *89* (1), 25–34. https://doi.org/10.1016/S0301-4622(00)00213-1.

(53) Rasband, W. ImageJ. *U. S. Natl. Institutes Heal. Bethesda, Maryland, USA* **2012**.

(54) Schneider, C. A.; Rasband, W. S.; Eliceiri, K. W. NIH Image to ImageJ: 25 Years of Image Analysis. *Nature Methods*. 2012. https://doi.org/10.1038/nmeth.2089.

(55) Kucharczyk, K.; Weiss, M.; Jastrzebska, K.; Luczak, M.; Ptak, A.; Kozak, M.; Mackiewicz, A.; Dams-Kozlowska, H. Bioengineering the Spider Silk Sequence to Modify Its Affinity for Drugs. *Int. J. Nanomedicine* **2018**. https://doi.org/10.2147/IJN.S168081.

(56) Safonova, L. A.; Bobrova, M. M.; Agapova, O. I.; Kotliarova, M. S.; Arkhipova, A. Y.; Moisenovich, M. M.; Agapov, I. I. Biological Properties of Regenerated Silk Fibroin Films. *Sovrem. Tehnol. v Med.* **2015**, *7* (3), 6–13. https://doi.org/10.17691/stm2015.7.3.01.

(57) Riss, T. L.; Moravec, R. A.; Niles, A. L.; Duellman, S.; Benink, H. A.; Worzella, T. J.; Minor, L. *Cell Viability Assays*; 2004.

(58) Kramschuster, A.; Turng, L. S. Fabrication of Tissue Engineering Scaffolds. In *Handbook of Biopolymers and Biodegradable Plastics: Properties, Processing and Applications*; 2012. https://doi.org/10.1016/B978-1-4557-2834-3.00017-3.

(59) Wang, Z.; Chen, W.; Cui, Z.; He, K.; Yu, W. Studies on Photoyellowing of Silk Fibroin and Alteration of Its Tyrosine Content. *J. Text. Inst.* **2016**. https://doi.org/10.1080/00405000.2015.1034933.

(60) Bucciarelli, A.; Chiera, S.; Quaranta, A.; Yadavalli, V. K.; Motta, A.; Maniglio, D. A Thermal-Reflow-Based Low-Temperature, High-Pressure Sintering of Lyophilized Silk Fibroin for the Fast Fabrication of Biosubstrates. *Adv. Funct. Mater.* **2019**, *1901134*, 1901134. https://doi.org/10.1002/adfm.201901134.

(61) Lin, H.; Zhang, D.; Alexander, P. G.; Yang, G.; Tan, J.; Cheng, A. W. M.; Tuan, R. S. Application of Visible Light-Based Projection Stereolithography for Live Cell-Scaffold Fabrication with Designed Architecture. *Biomaterials* **2013**. https://doi.org/10.1016/j.biomaterials.2012.09.048.

(62) Dubbin, K.; Tabet, A.; Heilshorn, S. C. Quantitative Criteria to Benchmark New and Existing Bio-Inks for Cell Compatibility. *Biofabrication* **2017**. https://doi.org/10.1088/1758-5090/aa869f.

(63) Sawicki, L. A.; Kloxin, A. M. Light-Mediated Formation and Patterning of Hydrogels for Cell Culture Applications. *J. Vis. Exp.* **2016**. https://doi.org/10.3791/54462.

(64) Holmes, R.; Yang, X. Bin; Dunne, A.; Florea, L.; Wood, D.; Tronci, G. Thiol-Ene Photo-Click Collagen-PEG Hydrogels: Impact of Water-Soluble Photoinitiators on Cell Viability, Gelation Kinetics and Rheological Properties. *Polymers (Basel).* **2017**. https://doi.org/10.3390/polym9060226.

(65) Wu, C.; Lim, J. Y.; Fuller, G. G.; Cegelski, L. Disruption of Escherichia Coli Amyloid-Integrated Biofilm Formation at the Air-Liquid Interface by a Polysorbate Surfactant. *Langmuir* **2013**. https://doi.org/10.1021/la304710k.

(66) Chou, D. K.; Krishnamurthy, R.; Randolph, T. W.; Carpenter, J. F.; Manning, M. C. Effects of Tween 20® and Tween 80® on the Stability of Albutropin during Agitation. *J. Pharm. Sci.* **2005**. https://doi.org/10.1002/jps.20365.

(67) Okino, S.; Ikeo, M.; Ueno, Y.; Taneda, D. Effects of Tween 80 on Cellulase Stability under Agitated Conditions. *Bioresour. Technol.* **2013**. https://doi.org/10.1016/j.biortech.2013.05.078.

(68) Kerwin, B. A. Polysorbates 20 and 80 Used in the Formulation of Protein Biotherapeutics: Structure and Degradation Pathways. *Journal of Pharmaceutical Sciences*. 2008. https://doi.org/10.1002/jps.21190.

(69) Scherzer, T.; Decker, U. Kinetic Investigations on the UV-Induced Photopolymerization of a Diacrylate by Time-Resolved FTIR Spectroscopy: The Influence of Photoinitiator Concentration, Light Intensity and Temperature. In *Radiation Physics and Chemistry*; 1999. https://doi.org/10.1016/S0969-806X(99)00257-1.

(70) García-Lizarribar, A.; Fernández-Garibay, X.; Velasco-Mallorquí, F.; Castaño, A. G.; Samitier,

J.; Ramon-Azcon, J. Composite Biomaterials as Long-Lasting Scaffolds for 3D Bioprinting of Highly Aligned Muscle Tissue. *Macromol. Biosci.* **2018**. https://doi.org/10.1002/mabi.201800167.

(71) Tian, S.; Ren, W.; Li, G.; Yang, R.; Wang, T. A Theoretical Analysis of Pore Size Distribution Effects on Shale Apparent Permeability. *Geofluids* **2017**. https://doi.org/10.1155/2017/7492328.

(72) MARSHALL, T. J. A RELATION BETWEEN PERMEABILITY AND SIZE DISTRIBUTION OF PORES. *J. Soil Sci.* **1958**. https://doi.org/10.1111/j.1365-2389.1958.tb01892.x.

(73) Mandal, B. B.; Grinberg, A.; Seok Gil, E.; Panilaitis, B.; Kaplan, D. L. High-Strength Silk Protein Scaffolds for Bone Repair. *Proc. Natl. Acad. Sci.* **2012**. https://doi.org/10.1073/pnas.1119474109.

(74) Rockwood, D. N.; Gil, E. S.; Park, S. H.; Kluge, J. A.; Grayson, W.; Bhumiratana, S.; Rajkhowa, R.; Wang, X.; Kim, S. J.; Vunjak-Novakovic, G.; et al. Ingrowth of Human Mesenchymal Stem Cells into Porous Silk Particle Reinforced Silk Composite Scaffolds: An in Vitro Study. *Acta Biomater.* **2011**. https://doi.org/10.1016/j.actbio.2010.07.020.

(75) Rajkhowa, R.; Gil, E. S.; Kluge, J.; Numata, K.; Wang, L.; Wang, X.; Kaplan, D. L. Reinforcing Silk Scaffolds with Silk Particles. *Macromol. Biosci.* **2010**. https://doi.org/10.1002/mabi.200900358.

(76) Gil, E. S.; Kluge, J. A.; Rockwood, D. N.; Rajkhowa, R.; Wang, L.; Wang, X.; Kaplan, D. L. Mechanical Improvements to Reinforced Porous Silk Scaffolds. *J. Biomed. Mater. Res. - Part A* **2011**. https://doi.org/10.1002/jbm.a.33158.

(77) Yodmuang, S.; McNamara, S. L.; Nover, A. B.; Mandal, B. B.; Agarwal, M.; Kelly, T. A. N.; Chao, P. H. G.; Hung, C.; Kaplan, D. L.; Vunjak-Novakovic, G. Silk Microfiber-Reinforced Silk Hydrogel Composites for Functional Cartilage Tissue Repair. *Acta Biomater.* **2015**. https://doi.org/10.1016/j.actbio.2014.09.032.

(78) Li, G.; Li, F.; Zheng, Z.; Luo, T.; Liu, J.; Wu, J.; Wang, X.; Kaplan, D. L. Silk Microfiber-Reinforced Silk Composite Scaffolds: Fabrication, Mechanical Properties, and Cytocompatibility. *J. Mater. Sci.* **2016**. https://doi.org/10.1007/s10853-015-9613-9.

(79) Gupta, P.; Adhikary, M.; M, J. C.; Kumar, M.; Bhardwaj, N.; Mandal, B. B. Biomimetic, Osteoconductive Non-Mulberry Silk Fiber Reinforced Tricomposite Scaffolds for Bone Tissue Engineering. *ACS Appl. Mater. Interfaces* **2016**. https://doi.org/10.1021/acsami.6b11366.

(80) Kesti, M.; Müller, M.; Becher, J.; Schnabelrauch, M.; D'Este, M.; Eglin, D.; Zenobi-Wong, M. A Versatile Bioink for Three-Dimensional Printing of Cellular Scaffolds Based on Thermally and Photo-Triggered Tandem Gelation. *Acta Biomater.* **2015**. https://doi.org/10.1016/j.actbio.2014.09.033.

(81) Linnenberger, A.; Bodine, M. I.; Fiedler, C.; Roberts, J. J.; Skaalure, S. C.; Quinn, J. P.; Bryant, S. J.; Cole, M.; McLeod, R. R. Three Dimensional Live Cell Lithography. *Opt. Express* **2013**. https://doi.org/10.1364/oe.21.010269.